Uplink Performance of Hardware-Impaired Cell-Free Massive MIMO with Multi-Antenna Users and Superimposed Pilots

Qiang Sun, *Member, IEEE*, Xiaodi Ji, Zhe Wang, Xiaomin Chen, *Member, IEEE*, Yongjie Yang, Jiayi Zhang, *Senior Member, IEEE*, Kai-Kit Wong, *Fellow, IEEE*

***Abstract*— Cell-free massive multiple-input multiple-output (mMIMO) has recently been proposed to improve cell edge performance. However, most prior works consider perfect hardware impairments (HIs), which are difficult to be achieved in practical systems. This paper studies the impact of HI in an uplink cell-free mMIMO system with both multi-antenna access points (APs) and multi-antenna user terminals (UTs) under the Weichselberger channel model.Firstly, we study a two-layer decoding scheme with local minimum mean-squared error or maximum ratio combining at the AP side and with optimal large-scale fading decoding in the central processing unit. We derive novel closed-form SE expressions and prove that the effect of HI can be mitigated in the case of UTs with multiple antennas. However, the achievable SE is constrained by the pilot contamination and pilot overhead. To this end, the superimposed pilot (SP) transmission method is considered in this paper, where all the coherence intervals are used for both pilot and data symbols transmission. Finally, numerical results verify our derived expressions and reveal the relationship between HI and the number of antennas per UT for different pilot schemes. Note that the advantages of SP over regular pilots disappear when the hardware quality decreases with multi-antenna UTs.**

***Index Terms*— Cell-free mMIMO, hardware impairments, superimposed pilot, linear combining, spectral efficiency.**

I. Introduction

With the development of wireless communication, cell-free massive multiple-input multiple-output (mMIMO) has attracted the interest of many researchers in the past few years and has been considered a promising wireless architecture for future communication systems [1]–[5]. In cell-free mMIMO systems, large numbers of access points (APs) and user terminals (UTs) are distributed randomly in a wide area, and all UTs are served concurrently by all APs connected to a central processing unit (CPU) via fronthaul links in the same resource block [2]. The distributed topology of cell-free mMIMO provides a macro-diversity gain, which significantly improves the spectral efficiency (SE) [2], [3], [6], [7]. Furthermore, a high degree of freedom can be available for the multi-antenna UTs that can provide spatial multiplexing [6], [7]. In addition, the authors proposed a two-layer decoding scheme, which is considered as a more practical and scalable decoding scheme [8]–[12]. At the AP side, various linear combining schemes (e.g., maximum ratio (MR) processing and local minimum mean-squared error (L-MMSE) combining) are used for suppressing interference. In the CPU, the large-scale fading decoding (LSFD) method is used for minimizing mean squared error in [9] and [10]. From the analytical view, an interesting novelty is that only statistical channel state information (CSI) is considered over the fronthaul links.

However, most works consider ideal hardware conditions at both the transceiver sides. In practice, most of the non-idealities (e.g., carrier-frequency offset, phase-noise, non-linearity of analog components, etc.) are considered in [13]–[15]. Although we can use high-quality hardware or complex signal processing methods to alleviate issues, these methods bring huge economic costs and energy consumption [16]. Hence, it is crucial to investigate the realistic cell-free mMIMO system with impaired-hardware components.

Analyzing the effect of HI on the cell-free mMIMO system has attracted the attention of many researchers [16]–[19]. In [16], the authors studied the typical HI model on the cell-free mMIMO system with single-antenna APs and single-antenna UTs and provided important insight that the influence of HI at the AP sides vanished gradually as the increasing number of APs. Furthermore, they presented a novel max-min power control algorithm to greatly enhance the performance of cell-free mMIMO systems. Similarly, reference [17] discussed the uplink of cell-free mMIMO systems with limited capacity fronthaul links and HI at both the transmitter and the receiver. Besides, the authors not only explored the effect of HI on the achievable SE of the cell-free mMIMO systems with multi-antenna APs and single-antenna UTs, but also presented different linear decoding schemes (i.e., LSFD, simple LSFD, simple centralized decoding, and small cell) in [18]. However, UTs in 5G networks have already been equipped with multiple antennas to exploit more spatial degree of freedom. We use the Weichselberger model for the scenario with multi-antenna UTs. It is important to investigate the effect of HI in such a practical deployment scenario and thus motivates our work.

This work was supported in part by National Natural Science Foundation of China under Grant 61971467, in part by the Key Research and Development Program of Jiangsu Province of China under Grant BE2021013-1, in part by the Qinlan Project of Jiangsu Province, in part by Natural Science Research Program of Nantong Vocational University under Grant 21ZK01, and in part by the Scientific Research Program of Nantong under Grant JC2021020. (Corresponding author: Yongjie Yang.)

Q. Sun, X. Ji, X. Chen, and Y. Yang are with the School of Information Science and Technology, Nantong University, Nantong 226019, China. (e-mail: sunqiang@ntu.edu.cn).

Z. Wang and J. Zhang are with the School of Electronic and Information Engineering, Beijing Jiaotong University, Beijing 100044, China. (e-mail: {zhewang_77@bjtu.edu.cn, jiayizhang}@bjtu.edu.cn).

K. Wong is with the Department of Electronic and Electrical Engineering, University College London, London, WC1E 7JE, United Kingdom.(e-mail: kai-kit.wong@ucl.ac.uk)

TABLE I
COMPARISON OF RELEVANT LITERATURE WITH THIS PAPER.

Ref.	Multi-antenna UTs	Joint correlation	HI	SP	LSFD	L-MMSE processing	Pilot contamination
[9]	✗	✗	✗	✗	✓	✓	✓
[18]	✗	✗	✓	✗	✓	✗	✓
[20]	✓	✓	✗	✗	✓	✓	✓
[34]	✗	✗	✗	✓	✗	✗	✓
[35]	✓	✗	✗	✗	✗	✓	✗
Proposed	✓	✓	✓	✓	✓	✓	✓

In addition, acquiring accurate channel state information (CSI) is particularly significant to detect the received signal at the APs. The coherence interval is the product of the coherence time and the coherence bandwidth over which the channel is relatively stable. In an uplink transmission phase, each AP performs channel estimation based on the orthogonal pilot sequences transmitted by the UTs in [20] and [21]. Only a fraction of the UTs can obtain orthogonal pilot sequences for channel estimation since the coherence interval has a constrained scale. However, when the number of UTs exceeds the number of pilot sequences, there will be some UTs using the same pilot sequences in a coherence interval. We also consider the pilot reuse, which degrades the performance in terms of channel estimation and SE due to the pilot contamination [22].

To minimize the effect of pilot contamination, researchers have investigated a variety of methods. In [23], [24], and [25], the authors exploit data covariance matrices or spatial channel correlation to design the pilot assignment scheme for reducing pilot contamination. Especially, the work in [24] indicated that the system capacity grows along with the increase of the number of antennas at the BS side when we use the independent covariance matrices of UTs reusing pilot sequences. Meanwhile, pilot assignment schemes have attracted much attention from many researchers, which allocated pilot sequences to all the UTs without altering the pilot structure [2], [22], [26]. In particular, the authors used a greedy pilot assignment scheme to enhance the minimum SE by renewing its standard pilot sequences in [2]. In addition, [26] has shown that the SE can be enhanced when the same pilot sequence can not be reused by contiguous UT, and [22] proposed a pilot assignment scheme to maximize the minimum distance between UTs that reused the same pilots.

However, in all the above-mentioned works, pilot training and data transmission are done separately in each coherent block, which is usually considered as regular pilot (RP) transmission. Reference [27] studied channel estimation and equalization based on a novelty transmission scheme, in which pilot sequences are hidden in the symbols. A growing number of researchers investigated an alternative transmission strategy, in which the pilot sequences and data signals are transmitted simultaneously [28]–[30]. We regard this strategy as superimposed pilot (SP) transmission, which can transmit pilot sequences in the whole coherence interval and mitigate pilot contamination by decreasing the possibility of pilot-reusing [31], [32]. SP transmission was considered for the uplink massive MIMO network [15], [33]. The authors derived the achievable closed-form SE and energy efficiency (EE) expressions with SP and indicated that SP has a comparable SE and EE to RP in a practical scenario [33]. Reference [34] studied the advantages of SP over RP in the cell-free mMIMO system. All the above works proved that the SP transmission method can achieve a higher achievable SE than RP. In addition, for multi-antenna UTs, it is better to transmit more orthogonal pilot sequences to reduce the influence of pilot contamination. Therefore, we consider the SP transmission scheme in the uplink cell-free mMIMO system with multi-antenna UTs.

Inspired by our observations from previous work, we investigate a hardware-impaired cell-free mMIMO system with multi-antenna APs and multi-antenna UTs and compare the system performance of two pilot transmission schemes (i.e., RP and SP). The comparisons of relevant literature with this paper are summarized in Table I. The primary contributions of our paper are as follows.

- We consider a cell-free mMIMO system with multi-antenna UTs in the presence of HI. We also investigate whether the effect of HI can be remitted in an uplink cell-free mMIMO system with multi-antenna UTs and whether the effect of HI at multi-antenna UTs is more than the one at multi-antenna APs. Results indicate that the achievable SE is affected obviously by the hardware imperfections at the multi-antenna UTs. It is recommended to implement low-quality hardware at the APs instead of UTs in the practical deployment.
- We use the SP transmission method for reducing pilot contamination in the case of multi-antenna UTs. Then we investigate the performance of SP in an uplink cell-free mMIMO system with multi-antenna UTs and compare the performance with RP. Results verify that SP outperforms RP in terms of the achievable SE without considering HI, and RP achieves higher performance gain when severe HI is considered. Therefore, it is not necessary to apply SP transmission in the scenario with severe HI.
- We analyze a two-layer decoding scheme first with L-MMSE or MR combining at the AP side and then with LSFD in the CPU (so-called Level 3 in [9]) for the scenario of multi-antenna UTs. This two-layer decoding scheme can minimize the mean squared error of the decoding signal and maximize the achievable SE. Besides, we derive novel closed-form SE expressions and

show that this two-layer decoding scheme with L-MMSE combining can maximize the achievable SE with HI in the presence of SP or RP.

The remainder of this paper is structured in the following order. In Section II, we consider a typical HI model for an uplink cell-free mMIMO system with multiple antennas at UTs and investigate different transmission periods with SP and RP, which include the pilot training, channel estimation, and uplink data transmission. In Section III, we derive the achievable SE with L-MMSE combining and novel closed-form SE expressions with MR combining receiver filters in different pilot transmission schemes. Then, Section IV exhibits numerical results. Finally, Section V gives a summary of this paper and a direction for future work.

Notation: Boldface lowercase letters $\mathbf{a}$ and boldface uppercase letters $\mathbf{A}$ represent column vectors and matrices. We use $(\mathbf{A})^*$, $(\mathbf{A})^T$ and $(\mathbf{A})^H$ to represent conjugate, transpose, and conjugate transpose, respectively. We use $\triangleq$ for definitions and $\mathbb{E}\{\cdot\}$ for the expectation operator. The determinant of a matrix is represented by $|\cdot|$. $\mathrm{vec}(\mathbf{A})$ is obtained by stacking of columns of matrix $\mathbf{A}$. The Kronecker products and the Hadamard products are indicated by $\otimes$ and $\odot$. $\mathbf{x} \sim \mathcal{N}_{\mathbb{C}}(0, \mathbf{R})$ denotes the circularly symmetric complex Gaussian distribution with zero mean and correlation matrix $\mathbf{R}$. $[\mathbf{A}]_n$ is the n-th column of $\mathbf{A}$.

II. System Model

In this paper, we consider a hardware-constrained cell-free mMIMO system consisting of M APs and K UTs randomly distributed in a large coverage area. Each AP is equipped with L antennas and each user has N antennas. In addition, all APs are connected to a CPU via fronthaul links, as shown in Fig.1. The channel between AP m and UT k is expressed by $\mathbf{H}_{mk} \in \mathbb{C}^{L\times N}$ which is a standard block fading model with τ_c time-frequency blocks. During the uplink transmission, the transmitted signal can be a pilot symbol or data symbol, or a combination of the pilot symbol and data symbol within a coherent interval. Therefore, we consider the two pilot transmission schemes, i.e., RP and SP in Fig.2. For the RP transmission, we use τ_p channel uses for the pilot training and $\tau_u = \tau_c - \tau_p$ channel uses for the data transmission, respectively. However, for the SP transmission, we use τ_c channel uses for the transmission of the pilot symbol and data symbol simultaneously. In this section, we describe the channel model, and when HI occurs, we further discuss the uplink transmission schemes with RP and SP.

A. The Weichselberger Rayleigh Channel Model

We consider the uplink channel based on the Weichselberger Rayleigh channel model [36], which is described as [20], [37]:

$$\mathbf{H}_{mk} = \mathbf{U}_{mk,\mathrm{r}} \left(\tilde{\mathbf{W}}_{mk} \odot \mathbf{G}_{mk,\mathrm{iid}} \right) \mathbf{U}_{mk,\mathrm{t}}^H, \tag{1}$$

where $\mathbf{G}_{mk,\mathrm{iid}} \in \mathbb{C}^{L\times N}$ is an independent and identically distributed $\mathcal{N}_{\mathbb{C}}(0,1)$ random variable, $\mathbf{U}_{mk,\mathrm{r}} \in \mathbb{C}^{L\times L}$ and $\mathbf{U}_{mk,\mathrm{t}} \in \mathbb{C}^{N\times N}$ represent the eigenvector matrices of the receiver and transmitter side correlation matrices $\mathbf{R}_{mk,\mathrm{r}} \triangleq \mathbb{E}[\mathbf{H}_{mk}\mathbf{H}_{mk}^H] \in \mathbb{C}^{L\times L}$ and $\mathbf{R}_{mk,\mathrm{t}} \triangleq \mathbb{E}[\mathbf{H}_{mk}^T\mathbf{H}_{mk}^*] \in \mathbb{C}^{N\times N}$, respectively. Besides, $\tilde{\mathbf{W}}_{mk}$ is the square root of each element of the spatially coupled matrix $\mathbf{W}_{mk}$ which indicates the spatial arrangement of scattering objects, and the (l,i)-th element $[\mathbf{W}_{mk}]_{li}$ denoting the average amount of power coupling from $\mathbf{u}_{mk,\mathrm{r},l}$ to $\mathbf{u}_{mk,\mathrm{t},i}$. Furthermore, $\mathbf{H}_{mk}$ can be reshaped as $\mathbf{H}_{mk} = [\mathbf{h}_{mk,1}; \cdots; \mathbf{h}_{mk,L}]$, where $\mathbf{h}_{mk,l}$ is the channel vector between UT k and l-th antenna of AP m. The channel $\mathbf{h}_{mk} = \mathrm{vec}(\mathbf{H}_{mk})$ and correlation matrix $\mathbf{R}_{mk} \triangleq \mathbb{E}[\mathbf{h}_{mk}\mathbf{h}_{mk}^H] \in \mathbb{C}^{LN\times LN}$ is written as [38]:

$$\mathbf{R}_{mk} = \left(\mathbf{U}_{mk,\mathrm{t}}^* \otimes \mathbf{U}_{mk,\mathrm{r}}\right) \mathrm{diag}\left(\mathrm{vec}(\mathbf{W}_{mk})\right) \left(\mathbf{U}_{mk,\mathrm{t}}^* \otimes \mathbf{U}_{mk,\mathrm{r}}\right)^H. \tag{2}$$

Remark 1: The Weichselberger model is suitable for the scenario with multi-antenna UEs, which not only considers the correlation features at both the AP-side and UE-side but models the joint correlation dependence between each AP-UE pair. I.I.D. Rayleigh fading channel is widely considered in previous articles. The channel model in Eq. (1) reduces to the uncorrelated Rayleigh fading channel when $\mathbf{W}_{mk}$ is given by

$$\mathbf{W}_{mk} = \beta_{mk} \mathbf{1}_{L\times N}. \tag{3}$$

Then, Eq. (1) will reduce to $\mathbf{H}_{mk} = \sqrt{\beta_{mk}}\mathbf{H}_{mk,\mathrm{iid}}$, and the results can also be easily derived. The Weichselberger model is more similar to the channel in actual deployment.

B. Hardware Impairments

In the ideal case, the transmitter sends a signal to the receiver through the channel, and the signal is only damaged

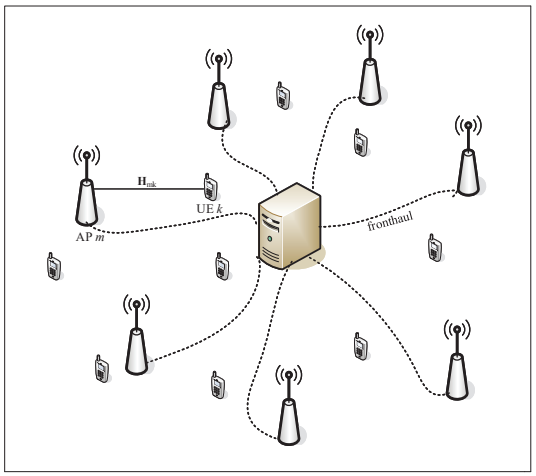

Fig. 1. Illustration of a cell-free mMIMO system.

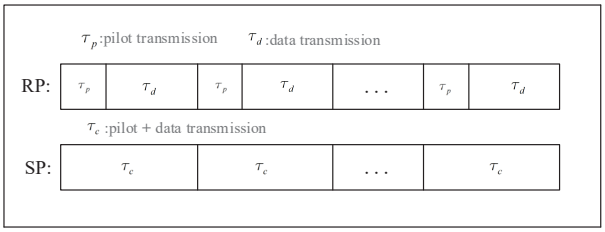

Fig. 2. Transmission protocol with RP and SP methods

by noise and channel fading [25]. Most existing works on cell-free mMIMO systems consider ideal transceiver hardware [8]–[10]. However, in practical scenarios, APs and UTs may suffer from low-quality hardware components (such as amplifiers and converters), resulting in signal distortion [13]–[15]. Different hardware distortion has different impacts on the system performance, and hardware imperfections are inevitable, whereas the extent of the impairments depends on hardware quality which has different costs or power consumption.

In this article, we use the basic model of HI. The distorted signal $\mathbf{y}$ is modeled by

$$\mathbf{y} = \sqrt{\kappa}\mathbf{x} + \boldsymbol{\eta}, \tag{4}$$

which denotes the input signal $\mathbf{x}$ to the hardware-impaired device. Meanwhile, the term $\kappa \in [0,1]$ represents the hardware quality coefficient, where 0 and 1 represent useless and perfect hardware components, respectively. The additive distortion term $\boldsymbol{\eta}$ is independent of the input signal $\mathbf{x}$, which also can be regarded as a kind of noise.

The transceiver HI can be represented by independent additive distortion noise at both the APs and UTs, which has been proved by extensive experiments in previous works [25]. Therefore, we analyze how these impairments affect SE for uplink transmission schemes with different pilot schemes in the following sections.

C. Uplink Transmission With RP

1) Channel Estimation: In this stage, all UTs transmit orthogonal pilot signals to the APs. Each AP will estimate the channels to all users by the uplink pilot signals. In each coherence interval, the length of the pilot training phase is τ_p. We use N orthogonal pilot sequences to form a matrix, which satisfies

$$\boldsymbol{\Phi}_l^H \boldsymbol{\Phi}_k = \begin{cases} \tau_p \mathbf{I}_N, & \text{if } l = k \\ 0. & \text{if } l \neq k \end{cases} \tag{5}$$

where $\tau_p \geq KN$ denotes that each UT can be assigned to a distinctive pilot matrix. But, the most case is $\tau_p \leq KN$ so that some UTs reuse the same pilot matrix (e.g., the k-th pilot matrix is reused by the UT set denoted by $\mathcal{P}_k \subset \{1, ..., K\}$).

Since we consider HI in such a system, the columns of the transmitter distortion matrix $\mathbf{J}_k^{UT} \in \mathbb{C}^{N\times\tau_p}$ follow independent circularly symmetric complex Gaussian distribution as $\boldsymbol{\eta}_k^{UT} \sim \mathcal{N}_{\mathbb{C}}\left(\mathbf{0}_N, (1-\kappa_t)\, p_k \mathbf{I}_N\right)$. For the receiver distortion matrix $\mathbf{P}_m^{AP} \in \mathbb{C}^{L\times\tau_p}$, its columns follow independent complex Gaussian distribution as $\boldsymbol{\eta}_m^{AP} \sim \mathcal{N}_{\mathbb{C}}\left(\mathbf{0}_L, \mathbf{D}_{m,\{h\}}\right)$, where $\mathbf{D}_{m,\{h\}} \triangleq (1-\kappa_r)\sum_{l=1}^{K} p_l \mathrm{diag}\left(\mathbf{h}_{ml,1}\mathbf{h}_{ml,1}^H, \cdots, \mathbf{h}_{ml,L}\mathbf{h}_{ml,L}^H\right)$. Then, the received signal $\mathbf{Y}_m^p \in \mathbb{C}^{L\times\tau_p}$ at AP m is

$$\mathbf{Y}_m^p = \sqrt{\kappa_r}\sum_{l=1}^{K} \mathbf{H}_{ml}\left(\sqrt{\hat{p}_l\kappa_t}\boldsymbol{\Omega}_l^{\frac{1}{2}}\boldsymbol{\Phi}_l^H + \mathbf{J}_l^{UT}\right) + \mathbf{P}_m^{AP} + \mathbf{N}_m, \tag{6}$$

where $\hat{p}_l$ is the pilot transmit power of UT l, $\boldsymbol{\Omega}_l = \mathrm{diag}\left\{\eta_{l1}^p, \ldots, \eta_{lN}^p\right\}$ is the power allocation matrix with $0 \leq \eta_{ln}^p \leq 1$ being the power allocation factor of the n-th antenna of UT l during the pilot transmission phase. In addition, $\mathbf{N}_m \in \mathbb{C}^{L\times\tau_p}$ is receiver noise whose elements are i.i.d. as $\mathcal{N}_{\mathbb{C}}(0,\sigma^2)$. To estimate channel accurately, we use the projection of $\mathbf{Y}_m^p$ onto $\boldsymbol{\Phi}_k/\sqrt{\tau_p}$ as

$$\mathbf{Y}_{mk}^p \triangleq \frac{\mathbf{Y}_m^p\boldsymbol{\Phi}_k}{\sqrt{\tau_p}} = \sqrt{\frac{\kappa_r}{\tau_p}}\sum_{l=1}^{K}\mathbf{H}_{ml}\left(\sqrt{\hat{p}_l\kappa_t}\boldsymbol{\Omega}_l^{\frac{1}{2}}\boldsymbol{\Phi}_l^H + \mathbf{J}_l^{UT}\right)\boldsymbol{\Phi}_k + \frac{\mathbf{P}_m^{AP}\boldsymbol{\Phi}_k}{\sqrt{\tau_p}} + \frac{\mathbf{N}_m\boldsymbol{\Phi}_k}{\sqrt{\tau_p}}, \tag{7}$$

where $\mathbf{E}_l^{UT} \triangleq \frac{\mathbf{J}_l^{UT}\boldsymbol{\Phi}_k}{\sqrt{\tau_p}}$, $\mathbf{F}_m^{AP} \triangleq \frac{\mathbf{P}_m^{AP}\boldsymbol{\Phi}_k}{\sqrt{\tau_p}}$ and $\mathbf{Q}_m \triangleq \frac{\mathbf{N}_m\boldsymbol{\Phi}_k}{\sqrt{\tau_p}}$. By making simplified process for $\mathbf{Y}_{mk}^p$, we derive

$$\mathbf{y}_{mk}^p = \mathrm{vec}\left(\mathbf{Y}_{mk}^p\right) = \sqrt{\kappa_r\kappa_t\tau_p}\sum_{l\in\mathcal{P}_k}\sqrt{\hat{p}_l}\left(\boldsymbol{\Omega}_l^{\frac{1}{2}}\otimes\mathbf{I}_L\right)\mathbf{h}_{ml} + \sqrt{\kappa_r}\sum_{l=1}^{K}\left(\mathbf{E}_l^{UT}\otimes\mathbf{I}_L\right)\mathbf{h}_{ml} + \mathrm{vec}\left(\mathbf{F}_m^{AP}\right) + \mathrm{vec}\left(\mathbf{Q}_m\right), \tag{8}$$

where $\tilde{\boldsymbol{\Omega}}_l^{\frac{1}{2}} \triangleq \boldsymbol{\Omega}_l^{\frac{1}{2}}\otimes\mathbf{I}_L$, $\mathbf{e}_l^{UT} \triangleq \mathbf{E}_l^{UT}\otimes\mathbf{I}_L$, $\mathbf{f}_m^{AP} = \mathrm{vec}\left(\mathbf{F}_m^{AP}\right)$ and $\mathbf{q}_m = \mathrm{vec}\left(\mathbf{Q}_m\right)$. With reference to estimation theory, the minimum mean-square error (MMSE) estimate of $\mathbf{h}_{mk}$ is

$$\hat{\mathbf{h}}_{mk} = \mathrm{vec}\left(\hat{\mathbf{H}}_{mk}\right) = \sqrt{\kappa_r\kappa_t\tau_p\hat{p}_k}\tilde{\boldsymbol{\Omega}}_l^{\frac{1}{2}}\mathbf{R}_{mk}\boldsymbol{\Psi}_{mk}^{-1}\mathbf{y}_{mk}^p, \tag{9}$$

where

$$\boldsymbol{\Psi}_{mk} = \mathbb{E}\left\{\mathbf{y}_{mk}^p\left(\mathbf{y}_{mk}^p\right)^H\right\} = \kappa_r\kappa_t\tau_p\sum_{l\in\mathcal{P}_k}\hat{p}_l\tilde{\boldsymbol{\Omega}}_l^{\frac{1}{2}}\mathbf{R}_{ml}\tilde{\boldsymbol{\Omega}}_l^{\frac{1}{2}} + \kappa_r\sum_{l=1}^{K}\mathbf{e}_l^{UT}\mathbf{R}_{ml}\left(\mathbf{e}_l^{UT}\right)^H + \mathbf{f}_m^{AP}\left(\mathbf{f}_m^{AP}\right)^H + \sigma^2\mathbf{I}_{LN}. \tag{10}$$

The channel estimation $\hat{\mathbf{h}}_{mk}$ and estimation error $\tilde{\mathbf{h}}_{mk} = \mathrm{vec}\left(\tilde{\mathbf{H}}_{mk}\right)$ follow independent circularly symmetric complex Gaussian distribution $\mathcal{N}_{\mathbb{C}}\left(0, \hat{\mathbf{R}}_{mk}\right)$ and $\mathcal{N}_{\mathbb{C}}\left(0, \mathbf{C}_{mk}\right)$, where

$$\hat{\mathbf{R}}_{mk} \triangleq \kappa_r\kappa_t\tau_p\hat{p}_k\tilde{\boldsymbol{\Omega}}_k^{\frac{1}{2}}\mathbf{R}_{mk}\boldsymbol{\Psi}_{mk}^{-1}\mathbf{R}_{mk}\tilde{\boldsymbol{\Omega}}_k^{\frac{1}{2}}, \tag{11}$$

$$\mathbf{C}_{mk} = \mathbf{R}_{mk} - \hat{\mathbf{R}}_{mk}. \tag{12}$$

2) Data Transmission: AP m receives a complex baseband signal which is expressed by

$$\mathbf{y}_m = \sqrt{\kappa_r}\sum_{l=1}^{K}\mathbf{H}_{ml}\left(\sqrt{\kappa_t}\mathbf{s}_l + \boldsymbol{\eta}_l^{UT}\right) + \boldsymbol{\eta}_m^{AP} + \mathbf{n}_m. \tag{13}$$

The UT k transmits signal $\mathbf{s}_k = \left[s_{k,1}, \cdots, s_{k,N}\right]^T$ which also can be represented as $\mathbf{s}_k = \sqrt{p_k}\mathbf{P}_k^{\frac{1}{2}}\mathbf{x}_k$, $\mathbf{x}_k$ is the transmitted data symbol of UT k, $\mathbf{P}_k = \mathrm{diag}\left\{\eta_{k1}^u, \ldots, \eta_{kN}^u\right\}$ is the power allocation matrix with $0 \leq \eta_{kn}^u \leq 1$ being the power control coefficient of the n-th antenna of UT k during the uplink data transmission phase, respectively. The transmitted signal power from UT k is p_k, and $\mathbf{n}_m \sim \mathcal{N}_{\mathbb{C}}(0, \sigma^2\mathbf{I}_L)$.

D. Uplink Transmission With SP

In the case of SP, we estimate CSI in the whole coherence interval τ_c. To acquire high-quality CSI, we can use the standard MMSE technique which is advocated to construct the receiver filters. In contrast to RP, the transmitter

$$\begin{aligned}\mathbf{\Psi}_{mk} = \mathbb{E}\left\{\mathbf{y}_{mk}^{SP}\left(\mathbf{y}_{mk}^{SP}\right)^H\right\} = \kappa_r\kappa_t\tau_c\sum_{l\in\mathcal{P}_k}\hat{p}_l\tilde{\mathbf{\Omega}}_l^{\frac{1}{2}}\mathbf{R}_{ml}\tilde{\mathbf{\Omega}}_l^{\frac{1}{2}} + \kappa_r\kappa_t\sum_{l=1}^{K}p_l\mathbf{e}\mathbf{x}_l^{UT}\mathbf{R}_{ml}\left(\mathbf{e}\mathbf{x}_l^{UT}\right)^H \\ + \kappa_r\sum_{l=1}^{K}\mathbf{e}_{l,\tau_p}^{SP}\mathbf{R}_{ml}\left(\mathbf{e}_{l,\tau_p}^{SP}\right)^H + \kappa_r\sum_{l=1}^{K}\mathbf{e}_{l,\tau_u}^{SP}\mathbf{R}_{ml}\left(\mathbf{e}_{l,\tau_u}^{SP}\right)^H + \mathbf{f}_m^{SP}\left(\mathbf{f}_m^{SP}\right)^H + \sigma^2\mathbf{I}_{LN}.\end{aligned} \tag{14}$$

$$\begin{aligned}\mathbf{Y}_{mk}^{SP} \triangleq \frac{\mathbf{Y}_m^{SP}\mathbf{\Phi}_k}{\sqrt{\tau_c}} = \sqrt{\kappa_r\kappa_t\tau_c}\sum_{l\in\mathcal{P}_k}\sqrt{\hat{p}_l}\mathbf{H}_{ml}\mathbf{\Omega}_l^{\frac{1}{2}} + \sqrt{\frac{\kappa_r\kappa_t}{\tau_c}}\sum_{l=1}^{K}\sqrt{p_l}\mathbf{H}_{ml}\mathbf{P}_l^{\frac{1}{2}}\mathbf{x}_l^H\mathbf{\Phi}_k + \sqrt{\frac{\kappa_r}{\tau_c}}\sum_{l=1}^{K}\mathbf{H}_{ml}\mathbf{J}_{l,\tau_p}^{SP}\mathbf{\Phi}_k \\ + \sqrt{\frac{\kappa_r}{\tau_c}}\sum_{l=1}^{K}\mathbf{H}_{ml}\mathbf{J}_{l,\tau_u}^{SP}\mathbf{\Phi}_k + \frac{\mathbf{P}_m^{SP}\mathbf{\Phi}_k}{\sqrt{\tau_c}} + \frac{\mathbf{N}_m^p\mathbf{\Phi}_k}{\sqrt{\tau_c}},\end{aligned} \tag{15}$$

distortions include the pilot sequence and data symbols of UT k. For a fraction of the pilot sequence, the transmitter distortion matrix is $\mathbf{J}_{k,\tau_p}^{SP} \in \mathbb{C}^{N\times\tau_p}$, whose columns are independently distributed as $\boldsymbol{\eta}_{k,\tau_p}^{UT} \sim \mathcal{N}_{\mathbb{C}}\left(\mathbf{0}_N, (1-\kappa_t)\,\hat{p}_k\mathbf{\Omega}_k\right)$. Similarly, for the data symbols, the transmitter distortion matrix is $\mathbf{J}_{k,\tau_u}^{SP} \in \mathbb{C}^{N\times\tau_p}$, whose columns follow independent circularly symmetric complex Gaussian distribution as $\boldsymbol{\eta}_{k,\tau_u}^{UT} \sim \mathcal{N}_{\mathbb{C}}\left(\mathbf{0}_N, (1-\kappa_t)\,p_k\mathbf{P}_k\right)$. For the receiver distortion matrix $\mathbf{P}_m^{SP} \in \mathbb{C}^{L\times\tau_p}$, whose columns follow independent complex Gaussian distribution as $\boldsymbol{\eta}_m^{SP} \sim \mathcal{N}_{\mathbb{C}}\left(\mathbf{0}_L, \mathbf{D}_{m,\{h\}}\right)$, where $\mathbf{D}_{m,\{h\}} \triangleq (1-\kappa_r)\sum_{l=1}^{K}(p_l+\hat{p}_l)\,\mathrm{diag}\left(\mathbf{h}_{ml,1}^H\mathbf{h}_{ml,1}, \cdots, \mathbf{h}_{ml,L}^H\mathbf{h}_{ml,L}\right)$.

In the case of SPs, all UTs transmit the combination of pilots and data symbols over the whole coherence block τ_c. Thus the received signal at AP m is given by

$$\begin{aligned}\mathbf{Y}_m^{SP} = \sqrt{\kappa_r}\sum_{l=1}^{K}\mathbf{H}_{ml}\Big(\sqrt{\hat{p}_l\kappa_t}\mathbf{\Omega}_l^{\frac{1}{2}}\mathbf{\Phi}_l^H + \sqrt{p_l\kappa_t}\mathbf{P}_l^{\frac{1}{2}}\mathbf{x}_l^H \\ + \mathbf{J}_{l,\tau_p}^{SP} + \mathbf{J}_{l,\tau_u}^{SP}\Big) + \mathbf{P}_m^{SP} + \mathbf{N}_m^p.\end{aligned} \tag{16}$$

In particular, to obtain accurate channel estimation, AP m firstly multiplies $\mathbf{Y}_m^{SP}$ with $\mathbf{\Phi}_k/\sqrt{\tau_p}$ to de-spread the received signal, which equals to Eq. (15) (see top of the page), where $\mathbf{E}\mathbf{X}_l^{UT} \triangleq \frac{\mathbf{P}_l^{\frac{1}{2}}\mathbf{x}_l^H\mathbf{\Phi}_k}{\sqrt{\tau_c}}, \mathbf{E}_{l,\tau_p}^{SP} \triangleq \frac{\mathbf{J}_{l,\tau_p}^{SP}\mathbf{\Phi}_k}{\sqrt{\tau_c}}, \mathbf{E}_{l,\tau_u}^{SP} \triangleq \frac{\mathbf{J}_{l,\tau_u}^{SP}\mathbf{\Phi}_k}{\sqrt{\tau_c}}, \mathbf{F}_m^{SP} \triangleq \frac{\mathbf{P}_m^{SP}\mathbf{\Phi}_k}{\sqrt{\tau_c}}$ and $\mathbf{Q}_m \triangleq \frac{\mathbf{N}_m^p\mathbf{\Phi}_k}{\sqrt{\tau_c}}$. By simplifying the processing procedure for $\mathbf{Y}_{mk}^{SP}$, we can have

$$\begin{aligned}\mathbf{y}_{mk}^{SP} = \mathrm{vec}\left(\mathbf{Y}_{mk}^{SP}\right) = \sqrt{\kappa_r\kappa_t\tau_c}\sum_{l\in\mathcal{P}_k}\sqrt{\hat{p}_l}\left(\mathbf{\Omega}_l^{\frac{1}{2}}\otimes\mathbf{I}_L\right)\mathbf{h}_{ml} \\ + \sqrt{\kappa_r\kappa_t}\sum_{l=1}^{K}\sqrt{p_l}\left(\mathbf{E}\mathbf{X}_l^{UT}\otimes\mathbf{I}_L\right)\mathbf{h}_{ml} + \sqrt{\kappa_r}\sum_{l=1}^{K}\left(\mathbf{E}_{l,\tau_p}^{SP}\otimes\mathbf{I}_L\right)\mathbf{h}_{ml} \\ + \sqrt{\kappa_r}\sum_{l=1}^{K}\left(\mathbf{E}_{l,\tau_u}^{SP}\otimes\mathbf{I}_L\right)\mathbf{h}_{ml} + \mathrm{vec}\left(\mathbf{Q}_m\right),\end{aligned} \tag{20}$$

where $\tilde{\mathbf{\Omega}}_l^{\frac{1}{2}} \triangleq \mathbf{\Omega}_l^{\frac{1}{2}}\otimes\mathbf{I}_L, \mathbf{e}\mathbf{x}_l^{UT} \triangleq \mathbf{E}\mathbf{X}_l^{UT}\otimes\mathbf{I}_L, \mathbf{e}_{l,\tau_p}^{SP} \triangleq \mathbf{E}_{l,\tau_p}^{SP}\otimes\mathbf{I}_L, \mathbf{e}_{l,\tau_u}^{SP} \triangleq \mathbf{E}_{l,\tau_u}^{SP}\otimes\mathbf{I}_L, \mathbf{f}_m^{SP} = \mathrm{vec}\left(\mathbf{F}_m^{SP}\right), \mathbf{q}_m = \mathrm{vec}\left(\mathbf{Q}_m\right)$. Then,

$$\begin{aligned}\mathbf{y}_{mk}^{SP} = \sqrt{\kappa_r\kappa_t\tau_c}\sum_{l\in\mathcal{P}_k}\sqrt{\hat{p}_l}\tilde{\mathbf{\Omega}}_l^{\frac{1}{2}}\mathbf{h}_{ml} + \sqrt{\kappa_r\kappa_t}\sum_{l=1}^{K}\sqrt{p_l}\mathbf{e}\mathbf{x}_l^{UT}\mathbf{h}_{ml} \\ + \sqrt{\kappa_r}\sum_{l=1}^{K}\mathbf{e}_{l,\tau_p}^{SP}\mathbf{h}_{ml} + \sqrt{\kappa_r}\sum_{l=1}^{K}\mathbf{e}_{l,\tau_u}^{SP}\mathbf{h}_{ml} + \mathbf{f}_m^{SP} + \mathbf{q}_m.\end{aligned} \tag{21}$$

The SP-based MMSE channel estimation is given by

$$\hat{\mathbf{h}}_{mk} = \mathrm{vec}\left(\hat{\mathbf{H}}_{mk}\right) = \sqrt{\kappa_r\kappa_t\tau_c\hat{p}_k}\tilde{\mathbf{\Omega}}_k^{\frac{1}{2}}\mathbf{R}_{mk}\mathbf{\Psi}_{mk}^{-1}\mathbf{y}_{mk}^{SP}, \tag{22}$$

where $\mathbf{\Psi}_{mk}$ as Eq. (14) (see top of the page).

In addition, the channel estimation $\hat{\mathbf{h}}_{mk}$ and the corresponding estimation error $\tilde{\mathbf{h}}_{mk} = \mathrm{vec}\left(\tilde{\mathbf{H}}_{mk}\right)$ respectively follow the distribution $\mathcal{N}_{\mathbb{C}}\left(0, \hat{\mathbf{R}}_{mk}\right)$ and $\mathcal{N}_{\mathbb{C}}\left(0, \mathbf{C}_{mk}\right)$, with $\hat{\mathbf{R}}_{mk} \triangleq \kappa_r\kappa_t\tau_c\hat{p}_k\tilde{\mathbf{\Omega}}_k^{\frac{1}{2}}\mathbf{R}_{mk}\mathbf{\Psi}_{mk}^{-1}\mathbf{R}_{mk}\tilde{\mathbf{\Omega}}_k^{\frac{1}{2}}$ and $\mathbf{C}_{mk} = \mathbf{R}_{mk} - \hat{\mathbf{R}}_{mk}$.

III. Uplink Achievable SE

In this section, we derive the achievable SE expressions for the two pilot transmission methods, i.e., RP and SP, and analyze a two-layer decoding scheme in that the local combining (i.e., L-MMSE combining or MR combining) is used at the AP side and the LSFD is used in the CPU for different pilot transmission schemes [9].

A. Achievable SE With RP

We assume that linear signal combining is used at the AP. Firstly, AP m selects the optimal linear receive combining matrix $\mathbf{V}_{mk} \in \mathbb{C}^{L\times N}$. Then, the local estimate of $\mathbf{s}_k$ obtained by

$$\begin{aligned}\tilde{\mathbf{s}}_{mk} = \mathbf{V}_{mk}^H\mathbf{y}_m = \sqrt{\kappa_r\kappa_t}\mathbf{V}_{mk}^H\mathbf{H}_{mk}\mathbf{s}_k + \sqrt{\kappa_r}\sum_{l=1}^{K}\mathbf{V}_{mk}^H\mathbf{H}_{ml}\boldsymbol{\eta}_l^{UT} \\ + \sqrt{\kappa_r\kappa_t}\sum_{l=1,l\neq k}^{K}\mathbf{V}_{mk}^H\mathbf{H}_{ml}\mathbf{s}_l + \mathbf{V}_{mk}^H\boldsymbol{\eta}_m^{AP} + \mathbf{V}_{mk}^H\mathbf{n}_m.\end{aligned} \tag{23}$$

In [9], we find that $\mathbf{V}_{mk}$ is related to local estimation $\hat{\mathbf{H}}_{mk}$. One possible choice is MR combining $\mathbf{V}_{mk} = \hat{\mathbf{H}}_{mk}$ that can

$$\hat{\mathbf{s}}_k = \sum_{m=1}^{M} \mathbf{A}_{mk}^H \tilde{\mathbf{s}}_{mk} = \sqrt{\kappa_r \kappa_t} \sum_{m=1}^{M} \mathbf{A}_{mk}^H \mathbf{V}_{mk}^H \mathbf{H}_{mk} \mathbf{s}_k + \sqrt{\kappa_r \kappa_t} \sum_{m=1}^{M} \sum_{l=1, l \neq k}^{K} \mathbf{A}_{mk}^H \mathbf{V}_{mk}^H \mathbf{H}_{ml} \mathbf{s}_l + \sqrt{\kappa_r} \sum_{m=1}^{M} \sum_{l=1}^{K} \mathbf{A}_{mk}^H \mathbf{V}_{mk}^H \mathbf{H}_{ml} \boldsymbol{\eta}_l^{UT} + \sum_{m=1}^{M} \mathbf{A}_{mk}^H \mathbf{V}_{mk}^H \boldsymbol{\eta}_m^{AP} + \sum_{m=1}^{M} \mathbf{A}_{mk}^H \mathbf{V}_{mk}^H \mathbf{n}_m, \tag{17}$$

$$\begin{aligned} \mathbf{D}_k &= \sqrt{\kappa_r \kappa_t p_k} \mathbf{A}_k^H \mathbb{E}\left\{\mathbf{G}_{kk}\right\} \mathbf{P}_k^{\frac{1}{2}} \\ \boldsymbol{\Sigma}_k &= \kappa_r \sum_{l=1}^{K} p_l \mathbf{A}_k^H \mathbb{E}\left\{\mathbf{G}_{kl} \mathbf{P}_l \mathbf{G}_{kl}^H\right\} \mathbf{A}_k - \mathbf{D}_k \mathbf{D}_k^H + \mathbf{A}_k^H \mathbf{F}_k \mathbf{A}_k + \mathbf{A}_k^H \mathbf{S}_k \mathbf{A}_k \\ \mathbf{F}_k &\triangleq \operatorname{diag}\left(\mathbb{E}\left\{\mathbf{V}_{1k}^H \mathbf{D}_{1,\{h\}} \mathbf{V}_{1k}\right\}; \cdots; \mathbb{E}\left\{\mathbf{V}_{Mk}^H \mathbf{D}_{M,\{h\}} \mathbf{V}_{Mk}\right\}\right) \end{aligned} \tag{18}$$

$$\mathrm{SE}_k = \left(1 - \frac{\tau_p}{\tau_c}\right) \log_2 \left| \mathbf{I}_N + \kappa_r \kappa_t p_k \mathbb{E}\left\{\mathbf{G}_{kk}^H\right\} \left(\kappa_r \sum_{l=1}^{K} p_l \mathbb{E}\left\{\mathbf{G}_{kl} \mathbf{P}_l \mathbf{G}_{kl}^H\right\} - \kappa_r \kappa_t p_k \mathbb{E}\left\{\mathbf{G}_{kk}\right\} \mathbf{P}_k \mathbb{E}\left\{\mathbf{G}_{kk}^H\right\} + \mathbf{F}_k + \sigma^2 \mathbf{S}_k \right)^{-1} \mathbb{E}\left\{\mathbf{G}_{kk}\right\} \mathbf{P}_k \right|. \tag{19}$$

obtain closed-form expression, and another one is L-MMSE combining matrix denoted as

$$\mathbf{V}_{mk} = \kappa_r \kappa_t p_k \left(\kappa_r \sum_{l=1}^{K} p_l \left(\hat{\mathbf{H}}_{ml} \mathbf{P}_l \hat{\mathbf{H}}_{ml}^H + \mathbf{C}'_{ml} \right) + \mathbf{D}_{m,\{h\}} + \sigma^2 \mathbf{I}_L \right)^{-1} \hat{\mathbf{H}}_{mk} \mathbf{P}_k. \tag{24}$$

Proof: The proof is presented in Appendix A. ∎

Then, the local estimates $\{\tilde{\mathbf{s}}_{mk} : m = 1, \cdots, M\}$ are sent to the CPU that uses LSFD coefficient matrix $\mathbf{A}_{mk}$ to obtain $\hat{\mathbf{s}}_k$ as as Eq. (34) (see top of the top page). We simplify the process by defining $\mathbf{A}_k \triangleq [\mathbf{A}_{1k}; \cdots; \mathbf{A}_{Mk}] \in \mathbb{C}^{MN \times N}$ and $\mathbf{G}_{kl} \triangleq \left[\mathbf{V}_{1k}^H \mathbf{H}_{1l}; \cdots; \mathbf{V}_{Mk}^H \mathbf{H}_{Ml}\right] \in \mathbb{C}^{MN \times N}$.

Finally, we can compute an uplink achievable SE of UT k for RP as the following corollary.

Corollary 1: For RP with MMSE-SIC detectors, an uplink achievable SE of UT k is

$$\mathrm{SE}_k = \left(1 - \frac{\tau_p}{\tau_c}\right) \log_2 \left| \mathbf{I}_N + \mathbf{D}_k^H \boldsymbol{\Sigma}_k^{-1} \mathbf{D}_k \right|, \tag{27}$$

where $\mathbf{D}_k$ and $\boldsymbol{\Sigma}_k$ are shown as Eq. (18) (see top of the page) and $\mathbf{S}_k \triangleq \operatorname{diag}\left(\mathbb{E}\left\{\mathbf{V}_{1k}^H \mathbf{V}_{1k}\right\}; \cdots; \mathbb{E}\left\{\mathbf{V}_{Mk}^H \mathbf{V}_{Mk}\right\}\right)$.

Proof: The proof is similar to that of [39] obeying the rules of matrix derivation, and hence we omit the proof procedure. ∎

Note that there is a pre-log factor in Eq. (27) due to only $\tau_c - \tau_p$ coherence interval used to transmit data symbols in the case of RP. We utilize L-MMSE combining matrix $\mathbf{V}_{mk}$ in Eq. (24) and LSFD coefficient matrix $\mathbf{A}_k$ to calculate the SE by using the method of Monte-Carlo. The complex LSFD coefficient matrix $\mathbf{A}_k$ can be designed by the CPU via the use of channel statistics as the following theorem.

Theorem 1: The uplink achievable SE of UT k is maximized by the complex LSFD coefficient matrix $\mathbf{A}_k$ as

$$\mathbf{A}_k = \kappa_r \kappa_t p_k \left(\kappa_r \sum_{l=1}^{K} p_l \mathbb{E}\left\{\mathbf{G}_{kl} \mathbf{P}_l \mathbf{G}_{kl}^H\right\} + \mathbf{F}_k + \sigma^2 \mathbf{S}_k \right)^{-1} \mathbb{E}\left\{\mathbf{G}_{kk}\right\} \mathbf{P}_k, \tag{28}$$

which results in the maximum SE as Eq. (19) (see top of the page).

Proof: The proof is similar to that in Appendix A, and we omit the proof procedure. ∎

Note that $\mathbf{A}_k$ can be optimized by the CPU in Eq. (28) which can maximize the uplink achievable SE in Eq. (19). If we adopt MR combining $\mathbf{V}_{mk} = \hat{\mathbf{H}}_{mk}$ at the AP side, we can obtain the closed-form SE expression as follows.

Theorem 2: The uplink achievable SE of UT k for MR combining $\mathbf{V}_{mk} = \hat{\mathbf{H}}_{mk}$ can be computed in closed-form as

$$\mathrm{SE}_k = \left(1 - \frac{\tau_p}{\tau_c}\right) \log_2 \left| \mathbf{I}_N + \mathbf{D}_k^H \boldsymbol{\Sigma}_k^{-1} \mathbf{D}_k \right|, \tag{29}$$

where $\mathbf{D}_k = \sqrt{\kappa_r \kappa_t p_k} \mathbf{A}_k^H \mathbf{T}_k \mathbf{P}_k^{\frac{1}{2}}$ and

$$\boldsymbol{\Sigma}_k = \mathbf{A}_k^H \left(\kappa_r \sum_{l=1}^{K} p_l \mathbf{Z}_{kl,(1)} + \kappa_r \sum_{l \in \mathcal{P}_k} p_l \mathbf{Z}_{kl,(2)} \right) \mathbf{A}_k - \mathbf{D}_k \mathbf{D}_k^H + \mathbf{A}_k^H \mathbf{F}_k \mathbf{A}_k + \sigma^2 \mathbf{A}_k^H \mathbf{S}_k \mathbf{A}_k, \tag{30}$$

with $\mathbf{T}_k = [\mathbf{T}_{1k}; \cdots; \mathbf{T}_{Mk}] \in \mathbb{C}^{MN \times N}$ and

$$\begin{aligned} \mathbf{S}_k &\triangleq \operatorname{diag}\left(\mathbb{E}\left\{\hat{\mathbf{H}}_{mk}^H \mathbf{V}_{1k}\right\}; \cdots; \mathbb{E}\left\{\hat{\mathbf{H}}_{mk}^H \mathbf{V}_{Mk}\right\}\right) \\ &= \operatorname{diag}\left(\mathbf{T}_{1k}; \cdots; \mathbf{T}_{Mk}\right), \end{aligned} \tag{31}$$

with the (n, n')-th element of $\mathbf{T}_{mk} \in \mathbb{C}^{N \times N}$ being $[\mathbf{T}_{mk}]_{nn'} = \mathbb{E}\left\{\hat{\mathbf{h}}_{mk,n}^H \hat{\mathbf{h}}_{mk,n'}\right\} = \operatorname{tr}\left(\hat{\mathbf{R}}_{mk}^{n'n}\right)$. Moreover, $\mathbf{Z}_{kl,(1)} = \operatorname{diag}\left(\left[\boldsymbol{\Gamma}_{1kl}^{(1)}, \cdots, \boldsymbol{\Gamma}_{Mkl}^{(1)}\right]\right)$ with the (n, n')-th element of $\boldsymbol{\Gamma}_{mkl}^{(1)} \in \mathbb{C}^{N \times N}$ being $\left[\boldsymbol{\Gamma}_{mkl}^{(1)}\right]_{nn'} =$

$$\begin{aligned}
&\mathbb{E}\left\{\hat{\mathbf{h}}_{mk,n}^H \mathbf{h}_{ml,i} \mathbf{h}_{ml,i}^H \hat{\mathbf{h}}_{mk,n'}\right\} \\
&= \kappa_r \kappa_t \tau_p p_k \operatorname{tr}\left(\mathbf{R}_{ml}^{ii} \mathbf{K}_{mkl,(1)}^{n'n}\right) + \kappa_r^2 \kappa_t^2 \tau_p^2 p_k p_l \sum_{z_1=1}^{N} \sum_{z_3=1}^{N} \operatorname{tr}\left(\tilde{\mathbf{K}}_{mkl,(2)}^{z_1 n} \tilde{\mathbf{R}}_{ml}^{iz_1}\right) \operatorname{tr}\left(\tilde{\mathbf{K}}_{mkl,(2)}^{n'z_3} \tilde{\mathbf{R}}_{ml}^{z_3 i}\right) \\
&+ \kappa_r^2 \kappa_t^2 \tau_p^2 p_k p_l \sum_{z_1=1}^{N} \sum_{z_2=1}^{N} \operatorname{tr}\left(\tilde{\mathbf{K}}_{mkl,(2)}^{z_1 n} \tilde{\mathbf{R}}_{ml}^{iz_2} \tilde{\mathbf{R}}_{ml}^{z_2 i} \tilde{\mathbf{K}}_{mkl,(2)}^{n'z_1}\right) + \kappa_r^2 \kappa_t \tau_p p_k \sum_{z_1=1}^{N} \sum_{z_2=1}^{N} \operatorname{tr}\left(\tilde{\mathbf{K}}_{mkl,(3)}^{z_1 n} \tilde{\mathbf{R}}_{ml}^{iz_2} \tilde{\mathbf{R}}_{ml}^{z_2 i} \tilde{\mathbf{K}}_{mkl,(3)}^{n'z_1}\right) \\
&+ \kappa_r^2 \kappa_t \tau_p p_k \sum_{z_1=1}^{N} \sum_{z_3=1}^{N} \operatorname{tr}\left(\tilde{\mathbf{K}}_{mkl,(3)}^{z_1 n} \tilde{\mathbf{R}}_{ml}^{iz_1}\right) \operatorname{tr}\left(\tilde{\mathbf{K}}_{mkl,(3)}^{n'z_3} \tilde{\mathbf{R}}_{ml}^{z_3 i}\right),
\end{aligned} \tag{25}$$

$$\begin{aligned}
&\mathbf{K}_{mkl,(1)} = \mathbb{E}\left\{\mathbf{S}_{mk} \mathbf{x}_{mk}^p \left(\mathbf{S}_{mk} \mathbf{x}_{mk}^p\right)^H\right\}, \mathbf{K}_{mkl,(2)} = \mathbb{E}\left\{\mathbf{S}_{mk} \tilde{\mathbf{\Omega}}_l^{\frac{1}{2}} \mathbf{h}_{ml} \left(\mathbf{S}_{mk} \tilde{\mathbf{\Omega}}_l^{\frac{1}{2}} \mathbf{h}_{ml}\right)^H\right\} = \mathbf{S}_{mk} \tilde{\mathbf{\Omega}}_l^{\frac{1}{2}} \mathbf{R}_{ml} \tilde{\mathbf{\Omega}}_l^{\frac{1}{2}} \mathbf{S}_{mk}^H, \\
&\mathbf{K}_{mkl,(3)} = \mathbb{E}\left\{\mathbf{S}_{mk} \mathbf{e}_l^{UT} \mathbf{h}_{ml} \left(\mathbf{S}_{mk} \mathbf{e}_l^{UT} \mathbf{h}_{ml}\right)^H\right\} = \mathbf{S}_{mk} \mathbf{e}_l^{UT} \mathbf{R}_{ml} \left(\mathbf{e}_l^{UT}\right)^H \mathbf{S}_{mk}^H.
\end{aligned} \tag{26}$$

$$\begin{aligned}
\mathbf{V}_{mk} = \kappa_r \kappa_t \Bigg(&\kappa_r \sum_{l=1}^{K} p_l \left(\hat{\mathbf{H}}_{ml} \mathbf{P}_l \hat{\mathbf{H}}_{ml}^H + \mathbf{C}'_{ml}\right) + \mathbf{D}_{m,\{h\}} + \kappa_r \sum_{l=1}^{K} \hat{p}_l \left(\hat{\mathbf{H}}_{ml} \mathbf{\Omega}_l \hat{\mathbf{H}}_{ml}^H + \tilde{\mathbf{H}}_{ml} \mathbf{\Omega}_l \tilde{\mathbf{H}}_{ml}^H\right) \\
&+ \sigma^2 \mathbf{I}_L \Bigg)^{-1} \left(p_k \hat{\mathbf{H}}_{mk} \mathbf{P}_k + \hat{p}_k \hat{\mathbf{H}}_{mk} \mathbf{\Omega}_k\right).
\end{aligned} \tag{32}$$

$$\begin{aligned}
\tilde{\mathbf{s}}_{mk} = \mathbf{V}_{mk}^H \mathbf{y}_{mj}^{SP} = &\sqrt{\kappa_r \kappa_t} \sum_{l=1}^{K} \sqrt{p_l} \mathbf{V}_{mk}^H \mathbf{H}_{ml} \mathbf{P}_l^{\frac{1}{2}} \left[\mathbf{x}_l^H\right]_j \sqrt{\kappa_r \kappa_t} \sum_{l=1}^{K} \sqrt{\hat{p}_l} \mathbf{V}_{mk}^H \mathbf{H}_{ml} \mathbf{\Omega}_l^{\frac{1}{2}} \left[\mathbf{\Phi}_l^H\right]_j + \mathbf{V}_{mk}^H \boldsymbol{\eta}_m^{SP} \\
&+ \sqrt{\kappa_r} \sum_{l=1}^{K} \mathbf{V}_{mk}^H \mathbf{H}_{ml} \boldsymbol{\eta}_{l,\tau_u}^{SP} + \sqrt{\kappa_r} \sum_{l=1}^{K} \mathbf{V}_{mk}^H \mathbf{H}_{ml} \boldsymbol{\eta}_{l,\tau_p}^{SP} + \mathbf{V}_{mk}^H \mathbf{n}_m.
\end{aligned} \tag{33}$$

$\sum_{i=1}^{N} \eta_{li} \operatorname{tr}\left(\mathbf{R}_{mk}^{ii} \hat{\mathbf{R}}_{mk}^{n'n}\right)$ and

$$\mathbf{Z}_{kl,(2)} = \begin{cases} \mathbf{\Gamma}_{1kl}^{(2)}, & m = M \\ \mathbf{\Pi}_{mkl} \mathbf{P}_l \mathbf{\Pi}_{M2lk}, & m \neq M \end{cases} \tag{36}$$

where the (n, n')-th element of $\mathbf{\Pi}_{mkl} \in \mathbb{C}^{N \times N}$ and $\mathbf{\Pi}_{m'kl} \in \mathbb{C}^{N \times N}$ is $[\mathbf{\Pi}_{mkl}]_{nn'} = \operatorname{tr}\left(\mathbf{\Upsilon}_{mkl}^{n'n}\right)$ and $[\mathbf{\Pi}_{m'lk}]_{nn'} = \operatorname{tr}\left(\mathbf{\Upsilon}_{m'lk}^{n'n}\right)$ respectively, $\mathbf{\Upsilon}_{mkl} \triangleq \mathbb{E}\left\{\hat{\mathbf{h}}_{ml} \hat{\mathbf{h}}_{mk}^H\right\} = \sqrt{\hat{p}_k \hat{p}_l} \kappa_r \kappa_t \tau_c \tilde{\mathbf{\Omega}}_l^{\frac{1}{2}} \mathbf{R}_{ml} \mathbf{\Psi}_{mk}^{-1} \mathbf{R}_{mk} \tilde{\mathbf{\Omega}}_k^{\frac{1}{2}}$, $\mathbf{\Upsilon}_{m'lk} \triangleq \mathbb{E}\left\{\hat{\mathbf{h}}_{m'k} \hat{\mathbf{h}}_{m'l}^H\right\} = \sqrt{\hat{p}_k \hat{p}_l} \kappa_r \kappa_t \tau_c \tilde{\mathbf{\Omega}}_k^{\frac{1}{2}} \mathbf{R}_{m'k} \mathbf{\Psi}_{m'k}^{-1} \mathbf{R}_{m'l} \tilde{\mathbf{\Omega}}_l^{\frac{1}{2}}$, $\left[\mathbf{\Gamma}_{mkl}^{(1)}\right]_{nn'} = \sum_{i=1}^{N} \eta_{li} \operatorname{tr}\left(\mathbf{R}_{mk}^{ii} \hat{\mathbf{R}}_{mk}^{n'n}\right)$, and $\left[\mathbf{\Gamma}_{mkl}^{(2)}\right]_{nn'} = \sum_{i=1}^{N} \eta_{li} \mathbb{E}\left\{\hat{\mathbf{h}}_{mk,n}^H \mathbf{h}_{ml,i} \quad \mathbf{h}_{ml,i}^H \hat{\mathbf{h}}_{mk,n'}\right\}$, the result of $\mathbb{E}\left\{\hat{\mathbf{h}}_{mk,n}^H \mathbf{h}_{ml,i} \mathbf{h}_{ml,i}^H \hat{\mathbf{h}}_{mk,n'}\right\}$ is shown in Eq. (25) and (26) (see top of the previous page). Besides, $\tilde{\mathbf{R}}_{ml}^{iz}, \tilde{\mathbf{K}}_{mk,(2)}^{nz}$ and $\tilde{\mathbf{K}}_{mkl,(3)}^{nz}$ are the submatrix of $\mathbf{R}_{ml}^{\frac{1}{2}}, \mathbf{K}_{mkl,(2)}^{\frac{1}{2}}$ and $\mathbf{K}_{mkl,(3)}^{\frac{1}{2}}$.

Proof: The proof is presented in Appendix B. ∎

Remark 2: The closed-form expression in (29) is generalized and concludes many specific situations which are discussed in Appendix B. This processing scheme has been extensively studied in existing work on massive MIMO with multi-antenna UTs but only considered idealistic hardware situations.

B. Achievable SE With SP

We combine the j^{th} column of $\mathbf{y}_m^{SP}$ with $\mathbf{V}_{mk}$ $(\forall j \in \{1, \cdots, \tau_c\})$, and obtain an estimation of the data symbol j transmitted by UT k as Eq. (33).

For any combining matrix, AP m uses its local estimate $\hat{\mathbf{H}}_{mk}$ to design $\mathbf{V}_{mk}$. Furthermore, the L-MMSE combining matrix is shown in Eq. (32).

Then, we use LSFD in the CPU. The local estimates $\{\tilde{\mathbf{s}}_{mk} : m = 1, \cdots, M\}$ are weighted by the LSFD coefficient matrix as Eq. (34).

Then, the achievable SE of UT k can be expressed as follows.

Corollary 2: The achievable SE of UT k for SP by using MMSE-SIC detectors is

$$\mathrm{SE}_k = \log_2 \left|\mathbf{I}_N + \mathbf{D}_k^H \mathbf{\Sigma}_k^{-1} \mathbf{D}_k\right|, \tag{37}$$

where $\mathbf{D}_k = \sqrt{\kappa_r \kappa_t p_k} \mathbf{A}_k^H \mathbb{E}\{\mathbf{G}_{kk}\} \mathbf{P}_k^{\frac{1}{2}}$ and

$$\begin{aligned}
\mathbf{\Sigma}_k = &\kappa_r \sum_{l=1}^{K} p_l \mathbf{A}_k^H \mathbb{E}\left\{\mathbf{G}_{kl} \mathbf{P}_l \mathbf{G}_{kl}^H\right\} \mathbf{A}_k - \mathbf{D}_k \mathbf{D}_k^H \\
&+ \kappa_r \sum_{l=1}^{K} \hat{p}_l \mathbf{A}_k^H \mathbb{E}\left\{\mathbf{G}_{kl} \mathbf{\Omega}_l \mathbf{G}_{kl}^H\right\} \mathbf{A}_k + \mathbf{A}_k^H \mathbf{F}_k \mathbf{A}_k + \mathbf{A}_k^H \mathbf{S}_k \mathbf{A}_k
\end{aligned}$$

Proof: The proof is similar to the one obeying the rules of matrix derivation in [39], and hence we omit the proof procedure. ∎

Note that there is no pre-log factor in Eq. (35) since the whole interval is used to transmit data symbols in the case of SP. However, the term $\mathbf{\Sigma}_k$ for SP increases the complexity of the SE expression due to the correlation between channel estimates and data symbols and accounts for the interference caused by the pilot and data symbols received from other UTs plus noise. In a similar way, the CPU only knows the channel

$$\hat{\mathbf{s}}_k = \sum_{m=1}^{M} \mathbf{A}_{mk}^H \tilde{\mathbf{s}}_{mk} = \sqrt{\kappa_r \kappa_t p_k} \sum_{m=1}^{M} \mathbf{A}_{mk}^H \mathbf{V}_{mk}^H \mathbf{H}_{mk} \mathbf{P}_k^{\frac{1}{2}} \left[\mathbf{x}_k^H\right]_j + \sqrt{\kappa_r \kappa_t} \sum_{m=1}^{M} \sum_{l=1, l\neq k}^{K} \sqrt{p_l} \mathbf{A}_{mk}^H \mathbf{V}_{mk}^H \mathbf{H}_{ml} \mathbf{P}_l^{\frac{1}{2}} \left[\mathbf{x}_l^H\right]_j + \sqrt{\kappa_r \kappa_t} \sum_{m=1}^{M} \sum_{l=1}^{K} \sqrt{\hat{p}_l} \mathbf{A}_{mk}^H \mathbf{V}_{mk}^H \mathbf{H}_{ml} \mathbf{\Omega}_l^{\frac{1}{2}} \left[\mathbf{\Phi}_l^H\right]_j + \sqrt{\kappa_r} \sum_{m=1}^{M} \sum_{l=1}^{K} \mathbf{A}_{mk}^H \mathbf{V}_{mk}^H \mathbf{H}_{ml} \boldsymbol{\eta}_{l,\tau_p}^{SP} + \sqrt{\kappa_r} \sum_{m=1}^{M} \sum_{l=1}^{K} \mathbf{A}_{mk}^H \mathbf{V}_{mk}^H \mathbf{H}_{ml} \boldsymbol{\eta}_{l,\tau_u}^{SP} + \sqrt{\kappa_r} \sum_{m=1}^{M} \mathbf{A}_{mk}^H \mathbf{V}_{mk}^H \boldsymbol{\eta}_m^{sp} + \sum_{m=1}^{M} \mathbf{A}_{mk}^H \mathbf{V}_{mk}^H \mathbf{n}_m. \tag{34}$$

$$\mathrm{SE}_k = \log_2 \left| \mathbf{I}_N + \kappa_r \kappa_t p_k \mathbb{E}\left\{\mathbf{G}_{kk}^H\right\} \left(\kappa_r \sum_{l=1}^{K} p_l \mathbb{E}\left\{\mathbf{G}_{kl} \mathbf{P}_l \mathbf{G}_{kl}^H\right\} - \kappa_r \kappa_t p_k \mathbb{E}\left\{\mathbf{G}_{kk}\right\} \mathbf{P}_k \mathbb{E}\left\{\mathbf{G}_{kk}^H\right\} + \kappa_r \sum_{l=1}^{K} \hat{p}_l \mathbb{E}\left\{\mathbf{G}_{kl} \mathbf{\Omega}_l \mathbf{G}_{kl}^H\right\} + \mathbf{F}_k + \sigma^2 \mathbf{S}_k \right)^{-1} \mathbb{E}\left\{\mathbf{G}_{kk}\right\} \mathbf{P}_k \right|. \tag{35}$$

statistic information, therefore, the complex LSFD coefficient matrix designed by the CPU for SP in Eq. (38) can also maximize the achievable rate of UT k as follows.

Theorem 3: The achievable SE of UT k for SP is maximized by using combing matrix $\mathbf{A}_k$ as

$$\mathbf{A}_k = \kappa_r \kappa_t \left(\kappa_r \sum_{l=1}^{K} p_l \mathbb{E}\{\mathbf{G}_{kl} \mathbf{P}_l \mathbf{G}_{kl}^H\} + \kappa_r \sum_{l=1}^{K} \hat{p}_l \mathbb{E}\{\mathbf{G}_{kl} \mathbf{\Omega}_l \mathbf{G}_{kl}^H\} + \mathbf{F}_k + \sigma^2 \mathbf{S}_k \right)^{-1} \left(p_k \mathbb{E}\left\{\mathbf{G}_{kk}\right\} \mathbf{P}_k + \hat{p}_k \mathbb{E}\left\{\mathbf{G}_{kk}\right\} \mathbf{\Omega}_k \right) \tag{38}$$

which results in the maximum SE as Eq. (35).

Proof: The proof is similar to that of Appendix A and we hence omit the proof procedure. ∎

Remark 3: L-MMSE combining is designed to maximize the SE at APs by using the local CSI, which can be adopted in RP and SP transmission. All the achievable SE expressions for RP and SP can be calculated by Monte Carlo methods. With regard to MR combining, we can not derive a closed-form expression of the achievable SE for SP due to the analytical intractability of the inverse matrix that contains the desired information and interference.

IV. Numerical Results

In this section, we quantitatively study the performance of hardware-impaired cell-free mMIMO with multi-antenna UTs over RP and SP. We consider that the L APs and K UTs are independently and randomly scattered within a square area of size 1 × 1 km. We expect that the APs can be deployed in environments with high user loads. The large-scale fading model contains path loss and shadow fading, and the large-scale fading coefficient is described by the COST 321 Walfish-Ikegami model as [40]:

$$\beta_{mk}[\mathrm{dB}] = -34.53 - 38 \log_{10}\left(d_{mk}/1\ \mathrm{m}\right) + F_{mk}, \tag{39}$$

where d_{mk} is the distance between AP m and UT k and F_{mk} represents the shadow fading. We assume the shadow fading with $F_{mk} = \sqrt{\delta_f} a_m + \sqrt{1-\delta_f} b_k$, where a_m and b_k satisfy the random distribution $\mathcal{N}\left(0, \delta_{\mathrm{sf}}^2\right)$ and $\mathcal{N}\left(0, \delta_{\mathrm{sf}}^2\right)$ respectively and δ_f is the shadow fading parameter. In all simulations, the important parameter settings are summarized in Table II, and other parameters are the same as those in [40].

TABLE II
System parameters for the simulation.

Parameter	Value
System bandwidth	20MHz
AP antenna height	12.65m
UT antenna heigh	1.65m
Receiver noise power	−94 dBm
δ_f	0.5
δ_{sf}	8dB

Each coherence block contains $\tau_c = 200$ samples. We set the length of pilot sequences τ_p with RP, which can form τ_p/N pilot matrix, so the pilot matrix of the first τ_p/N UTs is allocated randomly, and other UTs pick their pilot matrix that achieves the weakest interference to UTs in the current pilot set. The parameters p_k and $\hat{p}_k$ describe the transmit power of data and pilot symbols for UT k. Moreover, we define $p =$ 200mW as the total transmission energy per symbol, such that $p_k = \hat{p}_k = p$ with RP and $p_k + \hat{p}_k = p$ with SP.

We first compare the effects of HI for different combining schemes on cell-free mMIMO systems with multi-antenna UTs. Fig. 3 shows the cumulative distribution function (CDF) for the SE per UT over MR and L-MMSE combining when $M = 40$, $K = 10$, $L = 4$, $N = 4$, and HI coefficient factor $\kappa_t = \kappa_r = 0.997$. It can be clearly shown that L-MMSE combining is superior to MR combining since L-MMSE combining can make full use of all the antennas at AP to suppress interference. Furthermore, for MR combining, markers "○" formed by analytical results in (29) match perfectly with the Monte-Carlo simulation, which verifies our derived closed-form SE expressions.

Fig. 4 shows the CDF of the uplink average SE with different hardware quality factors in the transmitter and receiver. We can notice obviously that the parameters κ_r and κ_t have a different influence on the uplink average SE. For instance, at the

This article has been accepted for publication in IEEE Transactions on Communications. This is the author's version which has not been fully edited and content may change prior to final publication. Citation information: DOI 10.1109/TCOMM.2023.3301071

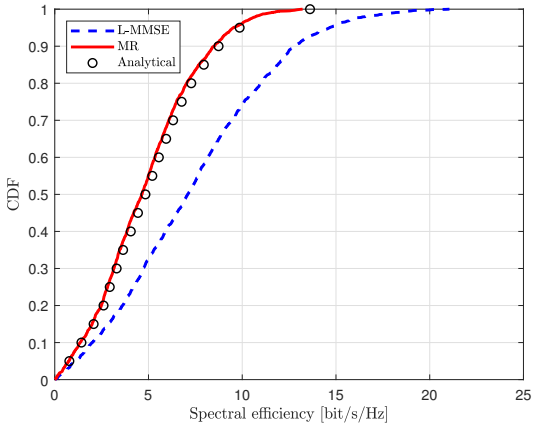

Fig. 3. CDF of the uplink SE with L-MMSE combining and MR combining over RP when $M = 40$, $K = 10$, $L = 4$, and $N = 4$.

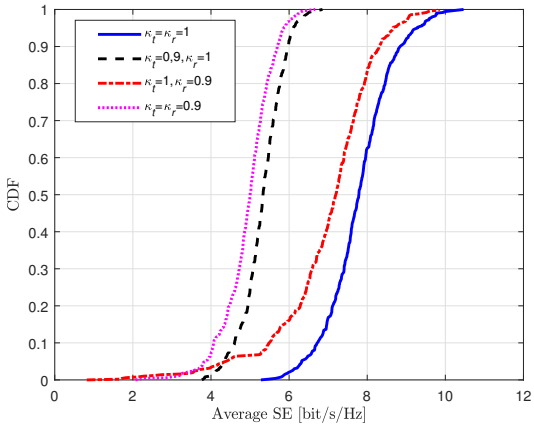

Fig. 4. CDF of the uplink average SE with L-MMSE combining for different values of κ_t and κ_r over RP when $M = 40$, $K = 10$, $L = 4$, and $N = 4$.

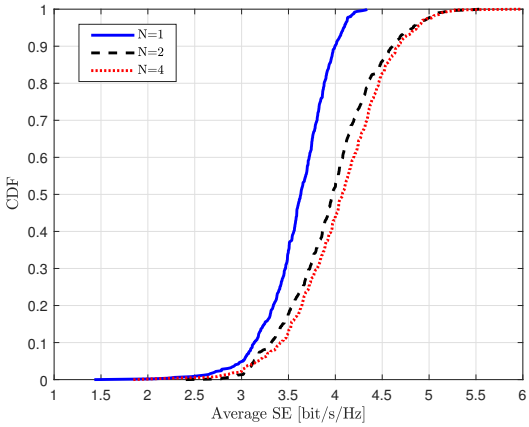

(a) L-MMSE combining

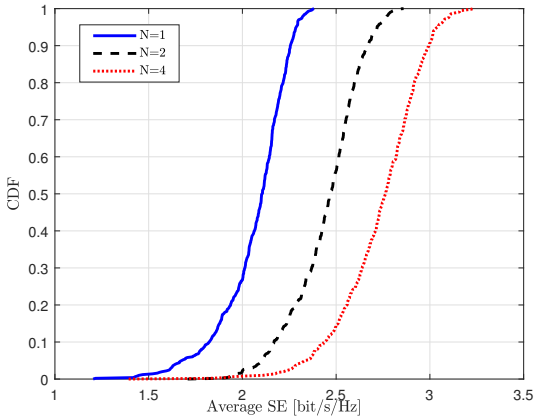

(b) MR combining

Fig. 5. CDF of the uplink average SE for different number of antennas N per UT with L-MMSE combining and MR combining over RP when $M = 40$, $K = 20$, $L = 4$, and $\kappa_t = \kappa_r = 0.997$.

90% likely SE points (i.e., the vertical axis is 0.1), the uplink average SE reduces by 18.07% when only κ_r decreases from 1 to 0.9. However, only κ_t reducing from 1 to 0.9 can cause a 31.69% average SE loss, which is close to the average SE loss for the case of $\kappa_r = \kappa_t = 0.9$. The achievable SE is affected obviously by the hardware imperfections at the multi-antenna UTs. To approach a better trade-off between performance and hardware costs, it is recommended to implement low-quality hardware at the APs instead of UTs.

Then, we explore the influence of the number of antennas per UT over HI. Fig. 5 plots the CDF of the uplink average SE for a different number of antennas N per UT over L-MMSE combining and MR combining when $M = 40$, $K = 20$, and $L = 4$. We can observe that the average SE increases linearly with the number of antennas per UT for MR combining, therefore, we can reduce the effects of HI by adding more antennas per UT. However, when using L-MMSE combining, the average SE of per-UT antennas $N = 2$ is close to that of per-UT antennas $N = 4$. From the results, we can observe that increasing the number of antennas per UT may not provide an improvement in SE. Thus, we can obtain the conclusion that the effects of HI can be alleviated for cell-free mMIMO systems with multiple antenna UTs and $N = 2$ is the optimal number of antennas per UT when considering the cost and performance improvement.

Fig. 6 shows the CDF of the achievable average SE against the number of antennas per UE N, for the same total number of UTs' antennas (i.e., $KN = 40$). We notice that the achievable average SE benefits from additional UE antennas in the case of the same total number of UTs' antennas. Compared with $K = 40$ and $N = 1$, the achievable average SE with $K = 10$ and $N = 4$ for L-MMSE combining and MR combining can achieve improvement greatly.

Next, we focus on the SE performance for different numbers of antennas N at the UT side over SP. The CDF as a function of the sum SE with MR combining and L-MMSE combining over SP against different antennas is shown in Fig. 7. We can find that all sum-SEs monotonously increase with N, and the performance gap between L-MMSE combining and MR combining undoubtedly become larger with the increase of N.

Fig. 8 compares the SE of SP and RP in the uplink cell-free mMIMO system when $M = 40$, $K = 20$, $L = 5$, and $N = 4$.

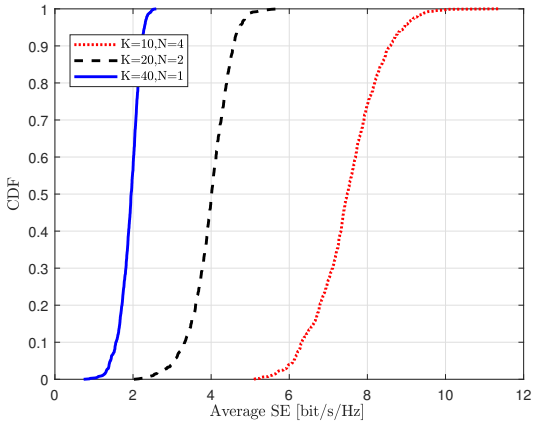

(a) L-MMSE combining

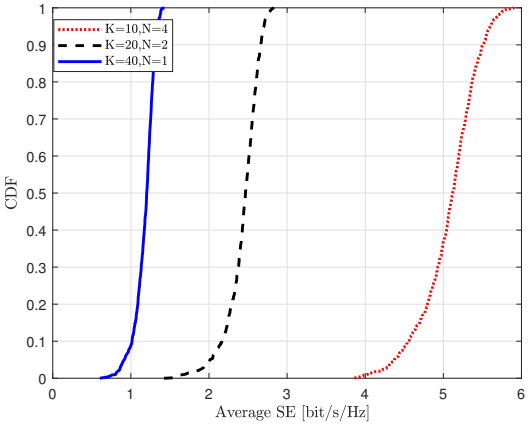

(b) MR combining

Fig. 6. CDF of the uplink average SE for the same total number of UTs' antennas with L-MMSE combining and MR combining over RP when $M = 40$, $L = 4$, $KN = 40$, and $\kappa_t = \kappa_r = 0.997$.

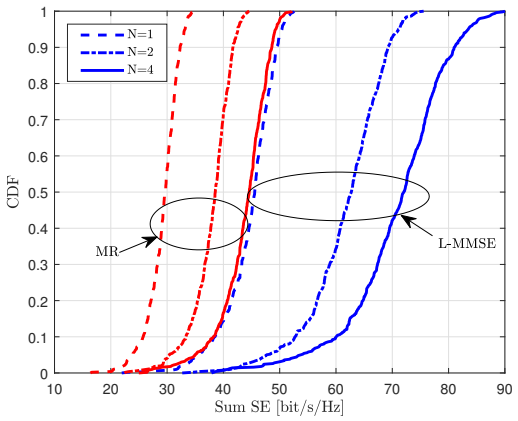

Fig. 7. CDF of the uplink sum SE for different number of antennas N per UT with L-MMSE combining and MR combining over SP when $M = 40$, $K = 20$, and $L = 5$.

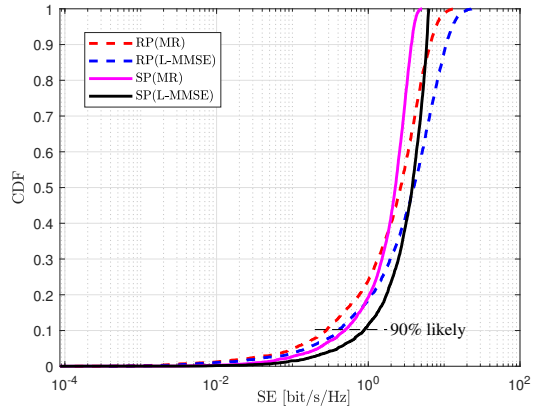

Fig. 8. CDF of the uplink SE with L-MMSE combining and MR combining over SP and RP when $M = 40$, $K = 20$, $L = 5$, and $N = 4$.

The figure plots the CDF as a function of the SE for L-MMSE combining and MR combining. At the 90% likely SE points (i.e., the vertical axis is 0.1), SP with L-MMSE combining and MR combining is significantly superior to RP since SP can help to suppress pilot contamination. In general, SP has a higher pre-log factor for RP, which can show a significant contribution in terms of achievable SE.

Fig.9 shows the achievable sum SE for SP and RP as functions of τ_c for L-MMSE combining and MR combining when $M = 40$, $L = 5$, $K = 20$, and $N = 4$. It is observed that the achievable sum SE for SP and RP have a significant improvement with the increasing of τ_c since a larger τ_c provides a higher pre-log factor for RP and more accurate channel estimation for SP.

Fig. 10 presents the sum SE as a function of the number of antennas per UT N with L-MMSE combining and MR combining over SP when $M = 40$, $K = [5\ 10\ 20]$, and $L = 5$. In terms of the sum SE, we observe that the L-MMSE combining method provides higher performance than the MR combining method. Besides, in the case of $K = 5$ or $K = 10$, the sum SE can be increased by about 106.05% and 79.79% respectively with L-MMSE combining by equipping with 5 antennas at the UT side when compared with $N = 1$. In the case of K=20, the sum SE decreases for a high number of antennas per UT due to the denominator term (i.e., cross-interference between the pilot sequences and data signals) increasing in Eq. (22), which greatly reduces the accuracy of channel estimation. Besides, the first term in the denominator (i.e., inter-user interference) increasing with the number of antennas in Eq. (35) results in the sum SE degradation.

Fig. 11 demonstrates the CDF of the uplink average SE for different HI factors over RP and SP when $M = 40$, $K = 10$, $L = 5$, and $N = 4$. Note that we use κ to describe hardware quality factor (i.e., $\kappa = \kappa_t = \kappa_r$). We find that RP achieves higher performance gain when severe hardware imperfections (such as $\kappa = 0.95$) are considered. The simultaneous transmission of pilot and data signals could accelerate the SE loss since severe transceiver imperfections are involved. Therefore, applying SP transmission in a scenario with severe hardware imperfection is unnecessary.

Fig. 12 compares the sum SE for different κ over different UT antennas N when $M = 40$, $K = 20$, and $L = 5$. We can

This article has been accepted for publication in IEEE Transactions on Communications. This is the author's version which has not been fully edited and content may change prior to final publication. Citation information: DOI 10.1109/TCOMM.2023.3301071

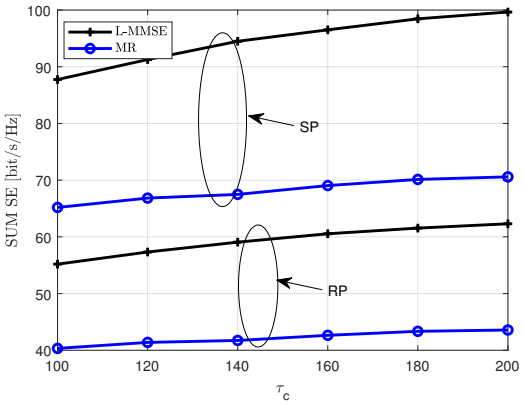

Fig. 9. The sum SE for L-MMSE combining and MR combining as a function of different τ_c over SP and RP when $M = 40$, $K = 20$, $L = 5$, and $N = 4$.

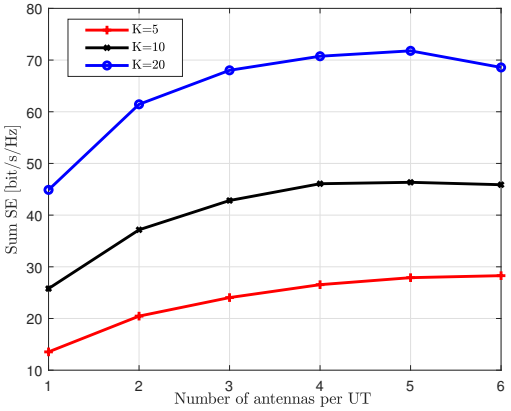

(a) L-MMSE combining

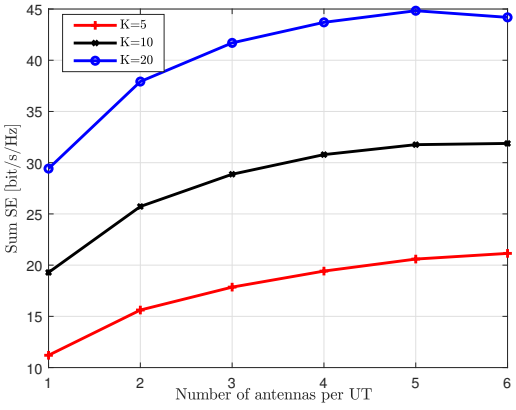

(b) MR combining

Fig. 10. The sum SE for L-MMSE combining and MR combining as a function of different number of antennas N per UT over SP when $M = 40$, $K = [5\ 10\ 20]$, and $L = 4$.

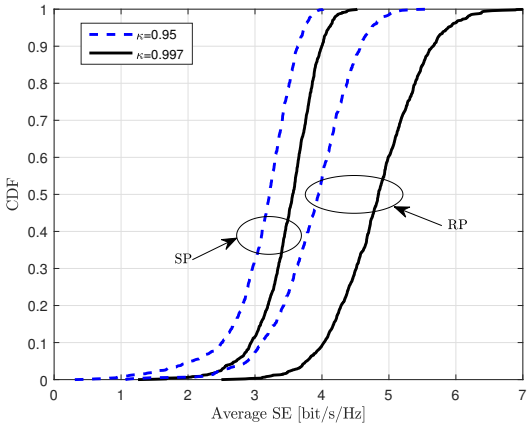

Fig. 11. CDF of the average SE for different κ with L-MMSE combining over SP and RP when $M = 40$, $K = 20$, $L = 5$, and $N = 4$.

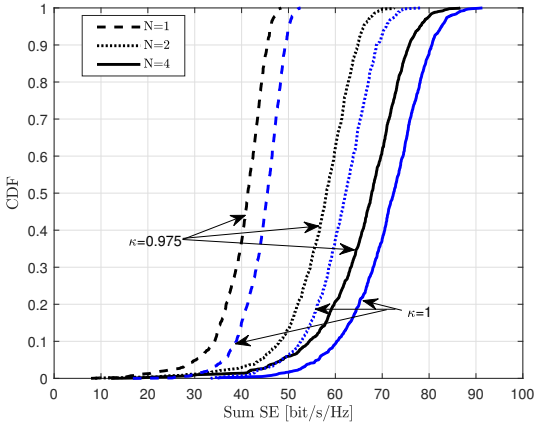

Fig. 12. CDF of the sum SE for different κ with different number of antennas N per UT over SP when $M = 40$, $K = 20$, and $L = 5$.

notice that the sum SE deteriorates with the decrease of κ and the sum SE increases greatly with the increase of N for the same κ. For example, the sum SE improves by 67.68% when the UT antenna N increases from 1 to 4 for $\kappa = 0.975$. The sum SE can be greatly improved with multi-antennas at UTs due to the increase of the spatial multiplexing gain in the case of different hardware quality.

V. Conclusions

In this paper, we have investigated the influence of HI on the performance of an uplink cell-free mMIMO system with both multi-antenna APs and multi-antenna UTs over the Weichselberger channel model. We computed the achievable SE expression with L-MMSE combining scheme and novel closed-form SE expression with MR combining at the AP side and optimal LSFD in the CPU. We found that increasing the number of antennas at the UT side can mitigate the effects of HI by increasing the spatial multiplexing gain. Then we considered a novel SP transmission method where all the coherence intervals are used for pilot matrix and data symbols transmission. We observed that the sum-SEs for SP were always superior to that of RP and the sum-SEs for SP were

improved with the increasing number of antennas per UT. However, the superiority of SP vanished when HI was severe in some practical scenarios. In future work, we will investigate more practical factors for the scenario of multi-antenna UTs in cell-free mMIMO systems and further optimize the system performance.

APPENDIX

A. Proof of L-MMSE combining Matrix (24)

According to [41], we can also represent the received signal $\mathbf{y}$ in (13) as

$$\begin{aligned}\mathbf{y} &= \sqrt{\kappa_r\kappa_t p_k}\hat{\mathbf{H}}_{mk}\mathbf{P}_k^{\frac{1}{2}}\mathbf{x}_k + \sqrt{\kappa_r\kappa_t p_k}\tilde{\mathbf{H}}_{mk}\mathbf{P}_k^{\frac{1}{2}}\mathbf{x}_k \\ &+ \sqrt{\kappa_r\kappa_t}\sum_{l\neq k}^{K}\sqrt{p_l}\hat{\mathbf{H}}_{ml}\mathbf{P}_l^{\frac{1}{2}}\mathbf{x}_l + \sqrt{\kappa_r\kappa_t}\sum_{l\neq k}^{K}\sqrt{p_l}\tilde{\mathbf{H}}_{ml}\mathbf{P}_l^{\frac{1}{2}}\mathbf{x}_l \\ &+ \sqrt{\kappa_r}\sum_{l=1}^{K}\hat{\mathbf{H}}_{ml}\boldsymbol{\eta}_l^{UT} + \sqrt{\kappa_r}\sum_{l=1}^{K}\tilde{\mathbf{H}}_{ml}\boldsymbol{\eta}_l^{UT} + \boldsymbol{\eta}_m^{AP} + \mathbf{n}_m.\end{aligned} \tag{40}$$

where

$$\begin{aligned}\mathbf{v} &\triangleq \sqrt{\kappa_r\kappa_t p_k}\tilde{\mathbf{H}}_{mk}\mathbf{P}_k^{\frac{1}{2}}\mathbf{x}_k + \sqrt{\kappa_r\kappa_t}\sum_{l\neq k}^{K}\sqrt{p_l}\hat{\mathbf{H}}_{ml}\mathbf{P}_l^{\frac{1}{2}}\mathbf{x}_l \\ &+ \sqrt{\kappa_r\kappa_t}\sum_{l\neq k}^{K}\sqrt{p_l}\tilde{\mathbf{H}}_{ml}\mathbf{P}_l^{\frac{1}{2}}\mathbf{x}_l + \sqrt{\kappa_r}\sum_{l=1}^{K}\hat{\mathbf{H}}_{ml}\boldsymbol{\eta}_l^{UT} \\ &+ \sqrt{\kappa_r}\sum_{l=1}^{K}\tilde{\mathbf{H}}_{ml}\boldsymbol{\eta}_l^{UT} + \boldsymbol{\eta}_m^{AP} + \mathbf{n}_m\end{aligned} \tag{41}$$

has an invertible covariance matrix

$$\begin{aligned}\boldsymbol{\Xi}_k &= \mathbb{E}\{\mathbf{v}\mathbf{v}^H|\hat{\mathbf{H}}_{mk}\} = \kappa_r\sum_{l=1}^{K}p_l\hat{\mathbf{H}}_{ml}\mathbf{P}_l\hat{\mathbf{H}}_{ml}^H \\ &-\kappa_r\kappa_t p_k\hat{\mathbf{H}}_{mk}\mathbf{P}_k\hat{\mathbf{H}}_{mk}^H + \kappa_r\sum_{l=1}^{K}p_l\mathbf{C}'_{ml} + \mathbf{D}_{m,\{h\}} + \sigma^2\mathbf{I}_N.\end{aligned} \tag{42}$$

To begin with, we multiply $\mathbf{y}$ with the invertible matrix $\boldsymbol{\Xi}_k^{-\frac{1}{2}}$:

$$\boldsymbol{\Xi}_k^{-\frac{1}{2}}\mathbf{y} = \sqrt{\kappa_r\kappa_t p_k}\boldsymbol{\Xi}_k^{-\frac{1}{2}}\hat{\mathbf{H}}_{mk}\mathbf{P}_k^{\frac{1}{2}}\mathbf{x}_k + \tilde{\mathbf{v}}, \tag{43}$$

where the noise $\tilde{\mathbf{v}} \triangleq \boldsymbol{\Xi}_k^{-\frac{1}{2}}\mathbf{v}$ becomes white. Next, we use the projection of (43) onto the $\sqrt{\kappa_r\kappa_t p_k}\boldsymbol{\Xi}_k^{-\frac{1}{2}}\hat{\mathbf{H}}_{mk}\mathbf{P}_k^{\frac{1}{2}}$ to obtain an effective channel

$$\begin{aligned}&\left(\sqrt{\kappa_r\kappa_t p_k}\boldsymbol{\Xi}_k^{-\frac{1}{2}}\hat{\mathbf{H}}_{mk}\mathbf{P}_k^{\frac{1}{2}}\right)^H\boldsymbol{\Xi}_k^{-\frac{1}{2}}\mathbf{y} \\ &= \kappa_r\kappa_t p_k\left(\hat{\mathbf{H}}_{mk}\mathbf{P}_k^{\frac{1}{2}}\right)^H\boldsymbol{\Xi}_k^{-1}\cdot\hat{\mathbf{H}}_{mk}\mathbf{P}_k^{\frac{1}{2}}\mathbf{x}_k \\ &+ \sqrt{\kappa_r\kappa_t p_k}\left(\hat{\mathbf{H}}_{mk}\mathbf{P}_k^{\frac{1}{2}}\right)^H\boldsymbol{\Xi}_k^{-1}\mathbf{v}.\end{aligned} \tag{44}$$

In the end, we can obtain the optimal combining matrix as

$$\begin{aligned}\mathbf{V}_{mk} &= \sqrt{\kappa_r\kappa_t p_k}\boldsymbol{\Xi}_k^{-1}\hat{\mathbf{H}}_{mk}\mathbf{P}_k^{\frac{1}{2}} \\ &= \sqrt{\kappa_r\kappa_t p_k}\left(\kappa_r\sum_{l=1}^{K}p_l\hat{\mathbf{H}}_{ml}\mathbf{P}_l\hat{\mathbf{H}}_{ml}^H - \kappa_r\kappa_t p_k\hat{\mathbf{H}}_{mk}\bar{\mathbf{P}}_k\hat{\mathbf{H}}_{mk}^H\right. \\ &\left.+\kappa_r\sum_{l=1}^{K}p_l\mathbf{C}'_{ml} + \mathbf{D}_{m,\{h\}} + \sigma^2\mathbf{I}_{ML}\right)^{-1}\hat{\mathbf{H}}_{mk}\mathbf{P}_k^{\frac{1}{2}}.\end{aligned} \tag{45}$$

Eq. (45) can be represented as the MMSE combining matrix and another scaling matrix [25] by the matrix inversion lemma. And the MMSE combining matrix denoted as

$$\begin{aligned}\mathbf{V}_{mk} &= \kappa_r\kappa_t p_k\left(\kappa_r\sum_{l=1}^{K}p_l\hat{\mathbf{H}}_{ml}\mathbf{P}_l\hat{\mathbf{H}}_{ml}^H + \mathbf{C}'_{ml} + \mathbf{D}_{m,\{h\}}\right. \\ &\left.+\sigma^2\mathbf{I}_{ML}\right)^{-1}\hat{\mathbf{H}}_{mk}\mathbf{P}_k\end{aligned} \tag{46}$$

maximizes the SE.

B. Proof of Theorem 2

We can derive the closed-form expression with MR combining. Firstly, we can compute the first part of Eq. (29) $\mathbf{D}_k = \sqrt{\kappa_r\kappa_t p_k}\mathbf{A}_k^H\mathbf{T}_k\mathbf{P}_k^{\frac{1}{2}}$ with $\mathbf{T}_k = [\mathbf{T}_{1k};\cdots;\mathbf{T}_{Mk}] \in \mathbb{C}^{MN\times N}$, where $\mathbf{T}_{mk} = \mathbb{E}\left\{\hat{\mathbf{H}}_{mk}^H\mathbf{H}_{mk}\right\} = \mathbb{E}\left\{\hat{\mathbf{H}}_{mk}^H\hat{\mathbf{H}}_{mk}\right\}$ and the (n,n')-th element of $\mathbf{T}_{mk}$ can be shown as $[\mathbf{T}_{mk}]_{nn'} = \mathbb{E}\{\hat{\mathbf{h}}_{mk,n}^H\hat{\mathbf{h}}_{mk,n'}\} = \mathrm{tr}(\hat{\mathbf{R}}_{mk}^{n'n})$. Then, we obtain the second part $\mathbf{S}_k$ as

$$\begin{aligned}\mathbf{S}_k &= \mathrm{diag}(\mathbb{E}\{\mathbf{V}_{1k}^H\mathbf{V}_{1k}\},\cdots,\mathbb{E}\{\mathbf{V}_{Mk}^H\mathbf{V}_{Mk}\}) \\ &= \mathrm{diag}(\mathbf{T}_{1k},\cdots,\mathbf{T}_{Mk}).\end{aligned} \tag{47}$$

The last part in the denominator the (m,m')-submatrix of $\mathbb{E}\{\mathbf{G}_{kl}\mathbf{P}_l\mathbf{G}_{kl}^H\}$ can be represented as $\mathbb{E}\{\mathbf{V}_{mk}^H\mathbf{H}_{ml}\mathbf{P}_l\mathbf{H}_{m'l}^H\mathbf{V}_{m'k}\}$. Then $\mathbb{E}\{\mathbf{V}_{mk}^H\mathbf{H}_{ml}\mathbf{P}_l\mathbf{H}_{m'l}^H\mathbf{V}_{m'k}\}$ can be computed exactly according to the following four cases.

Case 1: $m \neq m', l \notin \mathcal{P}_k$

$\mathbf{V}_{mk}$ and $\mathbf{H}_{ml}$ are statistically independent and both have mean 0 (i.e., combining of different APs and channels of different UTs). So $\mathbb{E}\{\mathbf{V}_{mk}^H\mathbf{H}_{ml}\mathbf{P}_l\mathbf{H}_{m'l}^H\mathbf{V}_{m'k}\} = 0$.

Case 2: $m \neq m', l \in \mathcal{P}_k$

$\mathbb{E}\{\mathbf{V}_{mk}^H\mathbf{H}_{ml}\mathbf{P}_l\mathbf{H}_{m'l}^H\mathbf{V}_{m'k}\} = \mathbb{E}\{\mathbf{V}_{mk}^H\mathbf{H}_{ml}\}\mathbf{P}_l\mathbb{E}\{\mathbf{H}_{m'l}^H\mathbf{V}_{m'k}\} = \boldsymbol{\Pi}_{mkl}\mathbf{P}_l\boldsymbol{\Pi}_{m'lk}$ while $\mathbb{E}\{\mathbf{V}_{mk}^H\mathbf{H}_{ml}\}$ and $\mathbb{E}\{\mathbf{H}_{m'l}^H\mathbf{V}_{m'k}\}$ are independent respectively. We can find that

$$\begin{aligned}\boldsymbol{\Pi}_{mkl} &= \mathbb{E}\left\{\mathbf{V}_{mk}^H\mathbf{H}_{ml}\right\} \\ &= \mathbb{E}\left\{\hat{\mathbf{H}}_{mk}^H\hat{\mathbf{H}}_{ml}\right\} = \begin{bmatrix}\mathrm{tr}\left(\boldsymbol{\Upsilon}_{mkl}^{11}\right) & \cdots & \mathrm{tr}\left(\boldsymbol{\Upsilon}_{mkl}^{N1}\right) \\ \vdots & \ddots & \vdots \\ \mathrm{tr}\left(\boldsymbol{\Upsilon}_{mkl}^{1N}\right) & \cdots & \mathrm{tr}\left(\boldsymbol{\Upsilon}_{mkl}^{NN}\right)\end{bmatrix},\end{aligned} \tag{48}$$

$$\begin{aligned}\boldsymbol{\Pi}_{m'lk} &= \mathbb{E}\left\{\mathbf{H}_{m'l}^H\mathbf{V}_{m'k}\right\} \\ &= \mathbb{E}\left\{\hat{\mathbf{H}}_{m'l}^H\hat{\mathbf{H}}_{m'k}\right\} = \begin{bmatrix}\mathrm{tr}\left(\boldsymbol{\Upsilon}_{m'lk}^{11}\right) & \cdots & \mathrm{tr}\left(\boldsymbol{\Upsilon}_{m'lk}^{N1}\right) \\ \vdots & \ddots & \vdots \\ \mathrm{tr}\left(\boldsymbol{\Upsilon}_{m'lk}^{1N}\right) & \cdots & \mathrm{tr}\left(\boldsymbol{\Upsilon}_{m'lk}^{NN}\right)\end{bmatrix},\end{aligned} \tag{49}$$

where

$$\begin{aligned}\mathbb{E}\left\{\left|\hat{\mathbf{h}}_{mk}^{H}\mathbf{h}_{ml}\right|^{2}\right\} &= \mathbb{E}\left\{\left|\mathbf{S}_{mk}^{H}\left(\mathbf{x}_{mk}^{p}+\sqrt{\kappa_r\kappa_t\tau_p p_l}\tilde{\mathbf{\Omega}}_{l}^{\frac{1}{2}}\mathbf{h}_{ml}+\sqrt{\kappa_r}\mathbf{e}_{l}^{UT}\mathbf{h}_{ml}\right)^{H}\mathbf{h}_{ml}\right|^{2}\right\}\\ &= \mathbb{E}\left\{\left|\left(\mathbf{S}_{mk}\mathbf{x}_{mk}^{p}\right)^{H}\mathbf{h}_{ml}\right|^{2}\right\}+\kappa_r\kappa_t\tau_p p_l\mathbb{E}\left\{\left|\left(\mathbf{S}_{mk}\tilde{\mathbf{\Omega}}_{l}^{\frac{1}{2}}\mathbf{h}_{ml}\right)^{H}\mathbf{h}_{ml}\right|^{2}\right\}+\kappa_r\mathbb{E}\left\{\left|\left(\mathbf{S}_{mk}\mathbf{e}_{l}^{UT}\mathbf{h}_{ml}\right)^{H}\mathbf{h}_{ml}\right|^{2}\right\}.\end{aligned} \tag{50}$$

$$\begin{aligned}\mathbf{K}_{mkl,(1)} &= \mathbb{E}\left\{\mathbf{S}_{mk}\mathbf{x}_{mk}^{p}\left(\mathbf{S}_{mk}\mathbf{x}_{mk}^{p}\right)^{H}\right\}=\mathbf{S}_{mk}\left(\mathbf{\Psi}_{mk}-\kappa_r\kappa_t\tau_p p_l\tilde{\mathbf{\Omega}}_{l}^{\frac{1}{2}}\mathbf{R}_{ml}\tilde{\mathbf{\Omega}}_{l}^{\frac{1}{2}}-\kappa_r\mathbf{e}_{l}^{UT}\mathbf{R}_{ml}\left(\mathbf{e}_{l}^{UT}\right)^{H}\right)\mathbf{S}_{mk}^{H},\\ \mathbf{K}_{mkl,(2)} &= \mathbb{E}\left\{\mathbf{S}_{mk}\tilde{\mathbf{\Omega}}_{l}^{\frac{1}{2}}\mathbf{h}_{ml}\left(\mathbf{S}_{mk}\tilde{\mathbf{\Omega}}_{l}^{\frac{1}{2}}\mathbf{h}_{ml}\right)^{H}\right\}=\mathbf{S}_{mk}\tilde{\mathbf{\Omega}}_{l}^{\frac{1}{2}}\mathbf{R}_{ml}\tilde{\mathbf{\Omega}}_{l}^{\frac{1}{2}}\mathbf{S}_{mk}^{H},\\ \mathbf{K}_{mkl,(3)} &= \mathbb{E}\left\{\mathbf{S}_{mk}\mathbf{e}_{l}^{UT}\mathbf{h}_{ml}\left(\mathbf{S}_{mk}\mathbf{e}_{l}^{UT}\mathbf{h}_{ml}\right)^{H}\right\}=\mathbf{S}_{mk}\mathbf{e}_{l}^{UT}\mathbf{R}_{ml}\left(\mathbf{e}_{l}^{UT}\right)^{H}\mathbf{S}_{mk}^{H}.\end{aligned} \tag{51}$$

$$\begin{aligned}\mathbf{\Upsilon}_{mkl} &\triangleq \mathbb{E}\left\{\hat{\mathbf{h}}_{ml}\hat{\mathbf{h}}_{mk}^{H}\right\}\\ &= \sqrt{\hat{p}_k\hat{p}_l}\kappa_r\kappa_t\tau_p\tilde{\mathbf{\Omega}}_{l}^{\frac{1}{2}}\mathbf{R}_{ml}\mathbf{\Psi}_{mk}^{-1}\mathbf{R}_{mk}\tilde{\mathbf{\Omega}}_{k}^{\frac{1}{2}},\end{aligned} \tag{52}$$

$$\begin{aligned}\mathbf{\Upsilon}_{m'kl} &\triangleq \mathbb{E}\left\{\hat{\mathbf{h}}_{m'k}\hat{\mathbf{h}}_{m'l}^{H}\right\}\\ &= \sqrt{\hat{p}_k\hat{p}_l}\kappa_r\kappa_t\tau_p\tilde{\mathbf{\Omega}}_{k}^{\frac{1}{2}}\mathbf{R}_{m'k}\mathbf{\Psi}_{m'k}^{-1}\mathbf{R}_{m'l}\tilde{\mathbf{\Omega}}_{l}^{\frac{1}{2}}.\end{aligned} \tag{53}$$

Case 3: $m=m', l\notin\mathcal{P}_k$

In this case, $\hat{\mathbf{H}}_{mk}$ and $\mathbf{H}_{ml}$ are incorrelated and $\mathbf{\Gamma}_{mkl}^{(1)}\triangleq\mathbb{E}\left\{\mathbf{V}_{mk}^{H}\mathbf{H}_{ml}\mathbf{P}_l\mathbf{H}_{ml}^{H}\mathbf{V}_{mk}\right\}=\mathbb{E}\left\{\hat{\mathbf{H}}_{mk}^{H}\mathbf{H}_{ml}\mathbf{P}_l\mathbf{H}_{ml}^{H}\hat{\mathbf{H}}_{mk}\right\}\in\mathbb{C}^{N\times N}$ whose (n,n')-th element can be represented as $[\mathbf{\Gamma}_{mkl}^{(1)}]_{nn'}=\sum_{i=1}^{N}\eta_{li}\mathbb{E}\{\hat{\mathbf{h}}_{mk,n}^{H}\mathbf{h}_{ml,i}\mathbf{h}_{ml,i}^{H}\hat{\mathbf{h}}_{mk,n'}\}$.

Due to the independence between $\hat{\mathbf{h}}_{mk}$ and $\mathbf{h}_{ml}$, we can get

$$\begin{aligned}&\mathbb{E}\left\{\hat{\mathbf{h}}_{mk,n}^{H}\mathbf{h}_{ml,i}\mathbf{h}_{ml,i}^{H}\hat{\mathbf{h}}_{mk,n'}\right\}\\ &=\mathrm{tr}\left(\mathbb{E}\left\{\mathbf{h}_{ml,i}\mathbf{h}_{ml,i}^{H}\right\}\mathbb{E}\left\{\hat{\mathbf{h}}_{mk,n'}\hat{\mathbf{h}}_{mk,n}^{H}\right\}\right)=\mathrm{tr}\left(\mathbf{R}_{ml}^{ii}\hat{\mathbf{R}}_{mk}^{n'n}\right)\end{aligned} \tag{54}$$

Then, we can obtain

$$\left[\mathbf{\Gamma}_{mkl}^{(1)}\right]_{nn'}=\sum_{i=1}^{N}\eta_{li}\mathrm{tr}\left(\mathbf{R}_{ml}^{ii}\hat{\mathbf{R}}_{mk}^{n'n}\right) \tag{55}$$

Case 4: $m=m', l\in\mathcal{P}_k$ In this instance, $\hat{\mathbf{H}}_{mk}$ and $\mathbf{H}_{ml}$ are not anymore independent and we make definitions that $\mathbf{\Gamma}_{mkl}^{(2)}\triangleq\mathbb{E}\{\mathbf{V}_{mk}^{H}\mathbf{H}_{ml}\mathbf{P}_l\mathbf{H}_{ml}^{H}\mathbf{V}_{mk}\}=\mathbb{E}\left\{\hat{\mathbf{H}}_{mk}^{H}\mathbf{H}_{ml}\mathbf{P}_l\mathbf{H}_{ml}^{H}\hat{\mathbf{H}}_{mk}\right\}$ whose (n,n')-th element is

$$\left[\mathbf{\Gamma}_{mkl}^{(2)}\right]_{nn'}=\sum_{i=1}^{N}\eta_{li}\mathbb{E}\left\{\hat{\mathbf{h}}_{mk,n}^{H}\mathbf{h}_{ml,i}\mathbf{h}_{ml,i}^{H}\hat{\mathbf{h}}_{mk,n'}\right\} \tag{56}$$

We notice that $\hat{\mathbf{h}}_{mk}$ and $\mathbf{h}_{ml}$ are not anymore independent. Similar to [42] and [35], let $\mathbf{x}_{mk}^{p}=\mathbf{y}_{mk}^{p}-\sqrt{\kappa_r\kappa_t\tau_p p_l}\tilde{\mathbf{\Omega}}_{l}^{\frac{1}{2}}\mathbf{h}_{ml}-\sqrt{\kappa_r}\mathbf{e}_{l}^{UT}\mathbf{h}_{ml}$ and $\mathbf{S}_{mk}=\tilde{\mathbf{\Omega}}_{k}^{\frac{1}{2}}\mathbf{R}_{mk}\mathbf{\Psi}_{mk}^{-1}$, so we can analyze $\mathbb{E}\{|\hat{\mathbf{h}}_{mk}^{H}\mathbf{h}_{ml}|^{2}\}$ as Eq. (50).

Note that $\mathbf{S}_{mk}\mathbf{x}_{mk}^{p}\sim\mathcal{N}_{\mathbb{C}}\left(\mathbf{0},\mathbf{K}_{mkl,(1)}\right)$, $\mathbf{S}_{mk}\tilde{\mathbf{\Omega}}_{l}^{\frac{1}{2}}\mathbf{h}_{ml}\sim\mathcal{N}_{\mathbb{C}}\left(\mathbf{0},\mathbf{K}_{mkl,(2)}\right)$ and $\mathbf{S}_{mk}\mathbf{e}_{l}^{UT}\mathbf{h}_{ml}\sim\mathcal{N}_{\mathbb{C}}\left(\mathbf{0},\mathbf{K}_{mkl,(3)}\right)$ where $\mathbf{K}_{mkl,(1)}$, $\mathbf{K}_{mkl,(2)}$ and $\mathbf{K}_{mkl,(3)}$ are shown in Eq. (51).

So we can rewrite $\mathbb{E}\{\hat{\mathbf{h}}_{mk,n}^{H}\mathbf{h}_{ml,i}\mathbf{h}_{ml,i}^{H}\hat{\mathbf{h}}_{mk,n'}\}$ as

$$\begin{aligned}&\mathbb{E}\left\{\hat{\mathbf{h}}_{mk,n}^{H}\mathbf{h}_{ml,i}\mathbf{h}_{ml,i}^{H}\hat{\mathbf{h}}_{mk,n'}\right\}\\ &=\kappa_r\kappa_t\tau_p p_k\mathbb{E}\left\{\left[\mathbf{S}_{mk}\mathbf{x}_{mk}^{p}\right]_{n}^{H}\mathbf{h}_{ml,i}\mathbf{h}_{ml,i}^{H}\left[\mathbf{S}_{mk}\mathbf{x}_{mk}^{p}\right]_{n'}\right\}+\\ &\kappa_r^2\kappa_t^2\tau_p^2 p_k p_l\mathbb{E}\left\{\left[\mathbf{S}_{mk}\tilde{\mathbf{\Omega}}_{l}^{\frac{1}{2}}\mathbf{h}_{ml}\right]_{n}^{H}\mathbf{h}_{ml,i}\mathbf{h}_{ml,i}^{H}\left[\mathbf{S}_{mk}\tilde{\mathbf{\Omega}}_{l}^{\frac{1}{2}}\mathbf{h}_{ml}\right]_{n'}\right\}\\ &+\kappa_r^2\kappa_t\tau_p p_k\mathbb{E}\left\{\left[\mathbf{S}_{mk}\mathbf{e}_{l}^{UT}\mathbf{h}_{ml}\right]_{n}^{H}\mathbf{h}_{ml,i}\mathbf{h}_{ml,i}^{H}\left[\mathbf{S}_{mk}\mathbf{e}_{l}^{UT}\mathbf{h}_{ml}\right]_{n'}\right\},\end{aligned} \tag{57}$$

where $[\mathbf{v}]_n$ is $\{(n-1)L+1\sim nL: n=1,\cdots,N\}$-th rows of $\mathbf{v}\in\mathbb{C}^{LN}$.

For the first part, since $\mathbf{S}_{mk}\mathbf{x}_{mk}^{\mathrm{p}}$ and $\mathbf{h}_{ml}$ are independent mutually, we can compute

$$\begin{aligned}&\mathbb{E}\left\{\left[\mathbf{S}_{mk}\mathbf{x}_{mk}^{p}\right]_{n}^{H}\mathbf{h}_{ml,i}\mathbf{h}_{ml,i}^{H}\left[\mathbf{S}_{mk}\mathbf{x}_{mk}^{p}\right]_{n'}\right\}\\ &=\mathrm{tr}\left(\mathbb{E}\left\{\mathbf{h}_{ml,i}\mathbf{h}_{ml,i}^{H}\right\}\mathbb{E}\left\{\left[\mathbf{S}_{mk}\mathbf{x}_{mk}^{\mathrm{p}}\right]_{n'}\left[\mathbf{S}_{mk}\mathbf{x}_{mk}^{\mathrm{p}}\right]_{n}^{H}\right\}\right)\\ &=\mathrm{tr}\left(\mathbf{R}_{ml}^{ii}\mathbf{K}_{mkl,(1)}^{n'n}\right).\end{aligned} \tag{58}$$

For the second part, we can indicate $[\mathbf{S}_{mk}\tilde{\mathbf{\Omega}}_{l}\mathbf{h}_{ml}]_{\{n,n'\}}$, $\left[\mathbf{S}_{mk}\mathbf{e}_{l}^{UT}\mathbf{h}_{ml}\right]_{\{n,n'\}}$ and $\mathbf{h}_{ml,\{i\}}$ into the equivalent form [35] as $[\mathbf{S}_{mk}\tilde{\mathbf{\Omega}}_{l}\mathbf{h}_{ml}]_{n}=\sum_{z=1}^{N}\tilde{\mathbf{K}}_{mkl,(2)}^{nz}\mathbf{q}_z$, $[\mathbf{S}_{mk}\tilde{\mathbf{\Omega}}_{l}\mathbf{h}_{ml}]_{n'}=\sum_{z=1}^{N}\tilde{\mathbf{K}}_{mkl,(2)}^{n'z}\mathbf{q}_z$,$[\mathbf{S}_{mk}\mathbf{e}_{l}^{UT}\mathbf{h}_{ml}]_{n}=\sum_{z=1}^{N}\tilde{\mathbf{K}}_{mkl,(3)}^{nz}\mathbf{q}_z$, $[\mathbf{S}_{mk}\mathbf{e}_{l}^{UT}\mathbf{h}_{ml}]_{n'}=\sum_{z=1}^{N}\tilde{\mathbf{K}}_{mkl,(3)}^{n'z}\mathbf{q}_z$ and $\mathbf{h}_{ml,i}=\sum_{z=1}^{N}\tilde{\mathbf{R}}_{ml}^{iz}\mathbf{q}_z$, respectively, where $\tilde{\mathbf{K}}_{mkl,(2)}^{nz}$ denotes the (n,z)-submatrix of $(\mathbf{K}_{mkl,(2)})^{\frac{1}{2}}$, $\tilde{\mathbf{K}}_{mkl,(3)}^{nz}$ denotes the (n,z)-submatrix of $(\mathbf{K}_{mkl,(3)})^{\frac{1}{2}}$, $\tilde{\mathbf{R}}_{ml}^{iz}$ denotes the (i,z)-submatrix of $\mathbf{R}_{ml}^{\frac{1}{2}}$ and $\mathbf{q}_z\sim\mathcal{N}_{\mathbb{C}}(\mathbf{0},\mathbf{I}_L)$, respectively. To simplify it, $\mathbf{h}_{ml}$ can be rewritten as

$$\begin{aligned}\mathbf{h}_{ml} &= \begin{bmatrix}\mathbf{h}_{ml,1}\\ \vdots\\ \mathbf{h}_{ml,N}\end{bmatrix}=\mathbf{R}_{ml}^{\frac{1}{2}}\begin{bmatrix}\mathbf{q}_1\\ \vdots\\ \mathbf{q}_N\end{bmatrix}\\ &= \begin{bmatrix}\tilde{\mathbf{R}}_{ml}^{11} & \cdots & \tilde{\mathbf{R}}_{ml}^{1N}\\ \vdots & \ddots & \vdots\\ \tilde{\mathbf{R}}_{ml}^{N1} & \cdots & \tilde{\mathbf{R}}_{ml}^{NN}\end{bmatrix}\begin{bmatrix}\mathbf{q}_1\\ \vdots\\ \mathbf{q}_N\end{bmatrix},\end{aligned} \tag{62}$$

and we also have $\mathbf{R}_{ml}^{ij}=\sum_{z=1}^{N}\tilde{\mathbf{R}}_{ml}^{iz}(\tilde{\mathbf{R}}_{ml}^{jz})^{H}=\sum_{z=1}^{N}\tilde{\mathbf{R}}_{ml}^{iz}\tilde{\mathbf{R}}_{ml}^{zj}$. So we can compute the second part as Eq.

$$\mathbb{E}\left\{\left[\mathbf{S}_{mk}\tilde{\mathbf{\Omega}}_l^{\frac{1}{2}}\mathbf{h}_{ml}\right]_n^H \mathbf{h}_{ml,i}\mathbf{h}_{ml,i}^H\left[\mathbf{S}_{mk}\tilde{\mathbf{\Omega}}_l^{\frac{1}{2}}\mathbf{h}_{ml}\right]_{n'}\right\}=\mathbb{E}\left\{\left(\sum_{z_1=1}^{N}\tilde{\mathbf{K}}_{mkl,(2)}^{nz_1}\mathbf{q}_{z_1}\right)^H\left(\sum_{z_2=1}^{N}\tilde{\mathbf{R}}_{ml}^{iz_2}\mathbf{q}_{z_2}\right)\left(\sum_{z_3=1}^{N}\tilde{\mathbf{R}}_{ml}^{iz_3}\mathbf{q}_{z_3}\right)^H\left(\sum_{z_4=1}^{N}\tilde{\mathbf{K}}_{mkl,(2)}^{n'z_4}\mathbf{q}_{z_4}\right)\right\}. \tag{59}$$

$$\mathbb{E}\left\{\left(\sum_{z_1=1}^{N}\mathbf{q}_{z_1}^H\tilde{\mathbf{K}}_{mkl,(2)}^{z_1n}\right)\left(\sum_{z_2=1}^{N}\tilde{\mathbf{R}}_{ml}^{iz_2}\mathbf{q}_{z_2}\mathbf{q}_{z_2}^H\tilde{\mathbf{R}}_{mkl,(2)}^{z_2i}\right)\left(\sum_{z_1=1}^{N}\tilde{\mathbf{K}}_{mkl,(2)}^{n'z_1}\mathbf{q}_{z_1}\right)\right\}=\sum_{z_1=1}^{N}\sum_{z_2=1}^{N}\mathrm{tr}\left(\tilde{\mathbf{K}}_{mkl,(2)}^{z_1n}\tilde{\mathbf{R}}_{ml}^{iz_2}\tilde{\mathbf{R}}_{ml}^{z_2i}\tilde{\mathbf{K}}_{mkl,(2)}^{n'z_1}\right). \tag{60}$$

$$\begin{aligned}\mathbb{E}\left\{\hat{\mathbf{h}}_{mk,n}^H\mathbf{h}_{ml,i}\mathbf{h}_{ml,i}^H\hat{\mathbf{h}}_{mk,n'}\right\}&=\kappa_r\kappa_t\tau_p p_k\mathrm{tr}\left(\mathbf{R}_{ml}^{ii}\mathbf{K}_{mkl,(1)}^{n'n}\right)\\&+\kappa_r^2\kappa_t^2\tau_p^2p_kp_l\sum_{z_1=1}^{N}\sum_{z_2=1}^{N}\mathrm{tr}\left(\tilde{\mathbf{K}}_{mkl,(2)}^{z_1n}\tilde{\mathbf{R}}_{ml}^{iz_2}\tilde{\mathbf{R}}_{ml}^{z_2i}\tilde{\mathbf{K}}_{mkl,(2)}^{n'z_1}\right)+\kappa_r^2\kappa_t^2\tau_p^2p_kp_l\sum_{z_1=1}^{N}\sum_{z_2=1}^{N}\mathrm{tr}\left(\tilde{\mathbf{K}}_{mkl,(2)}^{z_1n}\tilde{\mathbf{R}}_{ml}^{i'z_1}\right)\mathrm{tr}\left(\tilde{\mathbf{K}}_{mkl,(2)}^{n'z_2}\tilde{\mathbf{R}}_{ml}^{z_2i}\right)\\&+\kappa_r^2\kappa_t\tau_p p_k\sum_{z_1=1}^{N}\sum_{z_2=1}^{N}\mathrm{tr}\left(\tilde{\mathbf{K}}_{mkl,(3)}^{z_1n}\tilde{\mathbf{R}}_{ml}^{iz_2}\tilde{\mathbf{R}}_{ml}^{z_2i}\tilde{\mathbf{K}}_{mkl,(3)}^{n'z_1}\right)+\kappa_r^2\kappa_t\tau_p p_k\sum_{z_1=1}^{N}\sum_{z_2=1}^{N}\mathrm{tr}\left(\tilde{\mathbf{K}}_{mkl,(3)}^{z_1n}\tilde{\mathbf{R}}_{ml}^{i'z_1}\right)\mathrm{tr}\left(\tilde{\mathbf{K}}_{mkl,(3)}^{n'z_2}\tilde{\mathbf{R}}_{ml}^{z_2i}\right).\end{aligned} \tag{61}$$

(59). According to [35], if at least one of $z_j, j=1,\cdots 4$ is different from the others, (59) will be zero. If $z_1=z_2, z_3=z_4$ and $z_1=z_4, z_2=z_3$, (59) will be non-zero.

If $z_1=z_2, z_3=z_4$, (59) can be rewritten as

$$\begin{aligned}&\mathbb{E}\left\{\left(\sum_{z_1=1}^{N}\mathbf{q}_{z_1}^H\tilde{\mathbf{K}}_{mkl,(2)}^{z_1n}\tilde{\mathbf{R}}_{ml}^{iz_1}\mathbf{q}_{z_1}\right)\left(\sum_{z_3=1}^{N}\mathbf{q}_{z_3}^H\tilde{\mathbf{K}}_{mkl,(2)}^{z_3n'}\tilde{\mathbf{R}}_{ml}^{iz_3}\mathbf{q}_{z_3}\right)^H\right\}\\&=\sum_{z_1=1}^{N}\sum_{z_3=1}^{N}\mathrm{tr}\left(\tilde{\mathbf{K}}_{mkl,(2)}^{z_1n}\tilde{\mathbf{R}}_{ml}^{iz_1}\right)\mathrm{tr}\left(\tilde{\mathbf{K}}_{mkl,(2)}^{n'z_3}\tilde{\mathbf{R}}_{ml}^{z_3i}\right).\end{aligned} \tag{63}$$

If $z_1=z_4, z_2=z_3$, (59) can be rewritten as Eq. (60). So

$$\begin{aligned}&\mathbb{E}\left\{\left[\mathbf{S}_{mk}\tilde{\mathbf{\Omega}}_l^{\frac{1}{2}}\mathbf{h}_{ml}\right]_n^H\mathbf{h}_{ml,i}\mathbf{h}_{ml,i}^H\left[\mathbf{S}_{mk}\tilde{\mathbf{\Omega}}_l^{\frac{1}{2}}\mathbf{h}_{ml}\right]_{n'}\right\}\\&=\sum_{z_1=1}^{N}\sum_{z_2=1}^{N}\mathrm{tr}\left(\tilde{\mathbf{K}}_{mkl,(2)}^{z_1n}\tilde{\mathbf{R}}_{ml}^{iz_2}\tilde{\mathbf{R}}_{ml}^{z_2i}\tilde{\mathbf{K}}_{mkl,(2)}^{n'z_1}\right)\\&+\sum_{z_1=1}^{N}\sum_{z_3=1}^{N}\mathrm{tr}\left(\tilde{\mathbf{K}}_{mkl,(2)}^{z_1n}\tilde{\mathbf{R}}_{ml}^{iz_1}\right)\mathrm{tr}\left(\tilde{\mathbf{K}}_{mkl,(2)}^{n'z_3}\tilde{\mathbf{R}}_{ml}^{z_3i}\right).\end{aligned} \tag{64}$$

Similarly,

$$\begin{aligned}&\mathbb{E}\left\{\left[\mathbf{S}_{mk}\mathbf{e}_l^{UT}\mathbf{h}_{ml}\right]_n^H\mathbf{h}_{ml,i}\mathbf{h}_{ml,i}^H\left[\mathbf{S}_{mk}\mathbf{e}_l^{UT}\mathbf{h}_{ml}\right]_{n'}\right\}\\&=\sum_{z_1=1}^{N}\sum_{z_2=1}^{N}\mathrm{tr}\left(\tilde{\mathbf{K}}_{mkl,(3)}^{z_1n}\tilde{\mathbf{R}}_{ml}^{iz_2}\tilde{\mathbf{R}}_{ml}^{z_2i}\tilde{\mathbf{K}}_{mkl,(3)}^{n'z_1}\right)\\&+\sum_{z_1=1}^{N}\sum_{z_3=1}^{N}\mathrm{tr}\left(\tilde{\mathbf{K}}_{mkl,(3)}^{z_1n}\tilde{\mathbf{R}}_{ml}^{iz_1}\right)\mathrm{tr}\left(\tilde{\mathbf{K}}_{mkl,(3)}^{n'z_3}\tilde{\mathbf{R}}_{ml}^{z_3i}\right).\end{aligned} \tag{65}$$

To sum up, the above results are added into (57), we can obtain in Eq. (61).

In the end, we can have

$$\mathbb{E}_\mu\left\{\mathbf{G}_{kl}\mathbf{P}_l\mathbf{G}_{kl}^H\right\}=\begin{cases}\mathbf{Z}_{kl,(1)}, & l\notin\mathcal{P}_k\\ \mathbf{Z}_{kl,(2)}, & l\in\mathcal{P}_k\end{cases} \tag{66}$$

where $\mathbf{Z}_{kl,(1)}=\mathrm{diag}(\mathbf{\Gamma}_{1kl}^{(1)},\cdots,\mathbf{\Gamma}_{Mkl}^{(1)})$ and

$$\mathbf{Z}_{kl,(2)}=\begin{cases}\mathbf{\Gamma}_{1kl}^{(2)}, & m=M\\ \mathbf{\Pi}_{mkl}\mathbf{P}_l\mathbf{\Pi}_{M2lk}, & m\neq M\end{cases} \tag{67}$$

REFERENCES

[1] J. Zhang, E. Björnson, M. Matthaiou, D. W. K. Ng, H. Yang, and D. J. Love, "Prospective Multiple Antenna Technologies for Beyond 5G," *IEEE J. Sel. Areas Commun*, vol. 38, no. 8, pp. 1637-1660, Jun. 2020.

[2] H. Q. Ngo, A. Ashikhmin, H. Yang, E. G. Larsson, and T. L. Marzetta, "Cell-free massive MIMO versus small cells," *IEEE Trans. Wireless Commun.*, vol. 16, no. 3, pp. 1834–1850, Mar. 2017.

[3] S. Chen, J. Zhang, J. Zhang, E. Björnson, and B. Ai, "A survey on user-centric cell-free massive MIMO systems," *Digit. Commun. Netw.*, , 2021.

[4] J. Zhang, S. Chen, Y. Lin, J. Zheng, B. Ai, and L. Hanzo, "Cell-free massive MIMO: A new next-generation paradigm," *IEEE Access*, pp.99 878–99 888, 2019.

[5] S. Elhoushy, M. Ibrahim, and W. Hamouda "Cell-free massive MIMO: A survey," *IEEE Commun. Surveys Tuts.*, pp. 1–1, Oct. 2021.

[6] A. Adhikary, J. Nam, J. Ahn, and G. Caire "Joint spatial division and multiplexing–the large-scale array regime," *IEEE Trans. Inf. Theory.*, vol. 59, no. 10, pp. 6441–6463, Oct. 2013.

[7] E. Nayebi, A. Ashikhmin, T. L. Marzetta, H. Yang, and B. D. Rao, "Precoding and power optimization in cell-free massive MIMO systems," *IEEE Trans. Wireless Commun.*, vol. 16, no. 7, pp. 4445–4459, Jul. 2017.

[8] S. Buzzi, C. D'Andrea, A. Zappone, and C. D'Elia, "User-centric 5G cellular networks: Resource allocation and comparison with the cell-free massive MIMO approach," *IEEE Trans. Wireless Commun.*, vol. 19, no. 2, pp. 1250–1264, Feb. 2020.

[9] E. Björnson, and L. Sanguinetti, "Making cell-free massive MIMO competitive with MMSE processing and centralized implementation," *IEEE Trans. Wireless Commun.*, vol. 19, no. 1, pp. 77–90, Jan. 2019.

[10] J. Zheng, J. Zhang, L. Zhang, X. Zhang, and B. Ai, "On the total energy efficiency of cell-free massive MIMO," *IEEE Trans. Green Commun. Netw*, vol. 2, no. 1, pp. 25–39, Mar. 2018.

[11] J. Zhang, J. Zhang, D. W. K. Ng, S. Jin, and B. Ai, "Improving Sum-Rate of Cell-Free Massive MIMO with Expanded Compute-and-Forward," *IEEE Trans. Signal Process.*, vol. 70, pp. 202–215, 2022.

[12] J. Zhang, J. Zhang, E. Björnson, and B. Ai, "Local Partial Zero-Forcing Combining for Cell-Free Massive MIMO Systems," *IEEE Trans. Commun.*, vol. 69, no. 12, pp. 8459–8473, Dec. 2022.

[13] Q. Zhang, T. Q. Quek, and S. Jin, "Scaling analysis for massive MIMO systems with hardware impairments in Rician fading," *IEEE Trans. Wireless Commun.*, vol. 17, no. 7, pp. 4536–4549, Jul. 2018.

[14] C. Mollén and J. Choi and E. G. Larsson and R. W. Heath, Jr, "Uplink performance of wideband massive MIMO with one-bit ADCs," *IEEE Trans. Wireless Commun.*, vol. 16, no. 1, pp. 87–100, Jan. 2017.

[15] X. Gao, O. Edfors, F. Rusek, and F. Tufvesson, "Massive MIMO performance evaluation based on measured propagation data," *IEEE Trans. Wireless Commun.*, vol. 14, no. 7, pp. 3899–3911, Jul. 2015.

[16] J. Zhang, Y. Wei, E. Björnson, Y. Han, and S. Jin "Performance analysis and power control of cell-free massive MIMO systems with hardware impairments," *IEEE Access*, vol. 6, pp. 55 302–55 314, 2018

[17] H. Masoumi and M. J. Emadi, "Performance analysis of cell-free massive MIMO system with limited fronthaul capacity and hardware impairments," *IEEE Trans. Wireless Commun.*, vol. 19, no. 2, pp. 1038–1053, Feb. 2020.

[18] J. Zheng, J. Zhang, L. Zhang, X. Zhang, and B. Ai, "Efficient receiver design for uplink cell-free massive MIMO with hardware impairments," *IEEE Trans. Veh. Technol.*, vol. 69, no. 4, pp. 4537–4541, Apr. 2020.

[19] S. Elhoushy and W. Hamouda, "Performance of distributed massive MIMO and small-cell systems under hardware and channel impairments," *IEEE Trans. Veh. Technol.*, vol. 69, no. 8, pp. 8627–8642, Aug. 2020.

[20] Z. Wang, J. Zhang, B. Ai, C. Yuen, and M. Debbah, "Uplink Performance of Cell-Free Massive MIMO with Multi-Antenna Users Over Jointly-Correlated Rayleigh Fading Channels," *IEEE Trans. Wireless Commun.*, vol. 21, no. 9, pp. 7391–7406, Sep. 2022.

[21] Y. Jin, J. Zhang, S. Jin, and B. Ai, "Channel estimation for cell-free mmwave massive MIMO through deep learning," *IEEE Trans. Veh. Technol.*, vol. 68, no. 10, pp. 10 325–10 329, Oct. 2019.

[22] S. Buzzi, C. D'Andrea, M. Fresia, Y.-P. Zhang, and S. Feng, "Pilot assignment in cell-free massive MIMO based on the hungarian algorithm," *IEEE Wireless Commun. Lett.*, vol. 10, no. 1, pp. 34–37, Jan. 2021.

[23] H. Huh, G. Caire, H. C. Papadopoulos, and S. A. Ramprashad, "Achieving massive MIMO spectral efficiency with a not-so-large number of antennas," *IEEE Trans. Wireless Commun.*, vol. 11, no. 9, pp. 3226–3239, Sep. 2012.

[24] E. Björnson, J. Hoydis, and L. Sanguinetti, "Massive MIMO has unlimited capacitys," *IEEE Trans. Wireless Commun.*, vol. 17, no. 1, pp. 574–590, Jan. 2018.

[25] E. Björnson, J. Hoydis, and L. Sanguinetti, "Massive MIMO networks: Spectral, energy, and hardware efficiency," *Found. Trends Signal Process.*, vol. 11, no. 3-4, pp. 154–655, 2017.

[26] G. Interdonato, H. Q. Ngo, P. Frenger, and E. G. Larsson, "Downlink training in cell-free Massive MIMO: A blessing in disguise," *IEEE Trans. Wireless Commun.*, vol. 18, no. 11, pp. 5153–5169, Aug. 2019.

[27] F. Mazzenga, "Channel estimation and equalization for M-QAM transmission with a hidden pilot sequence," *IEEE Trans. Broadcast.*, vol. 46, no. 2, pp. 170–176, Jun. 2000.

[28] S. T. A. Goljahani, N. Benvenuto and L. Vangelista, "Superimposed sequence versus pilot aided channel estimations for next generation DVB-T systems," *IEEE Trans. Veh. Technol.*, vol. 55, no. 1, pp. 140–144, Mar. 2009.

[29] G. Interdonato, H. Q. Ngo, P. Frenger, and E. G. Larsson, "On the power allocation and system capacity of OFDM systems using superimposed training schemes," *IEEE Trans. Veh. Technol.*, vol. 58, no. 4, p. 1731–1740, May. 2009.

[30] N. Chen and G. T. Zhou, "Superimposed training for OFDM: A peak-to-average power ratio analysis," *IEEE Trans. Signal Process.*, vol. 54, no. 6, p. 2277–2287, Jun. 2006.

[31] H. Liu, J. Zhang, S. Jin, and B. Ai, "Graph coloring based pilot assignment for cell-free massive MIMO systems," *IEEE Trans. Veh. Technol.*, vol. 69, no. 8, pp. 9180–9184, Aug. 2020.

[32] H. Liu, J. Zhang, X. Zhang, A. Kurniawan, T. Juhana, and B. Ai, "Tabu-search-based pilot assignment for cell-free massive MIMO systems," *IEEE Trans. Veh. Technol.*, vol. 69, no. 2, pp. 2286–2290, Feb. 2020.

[33] D. Verenzuela, E. Björnson, and L. Sanguinetti, "Spectral and energy efficiency of superimposed pilots in uplink massive MIMO," *IEEE Trans. Wireless Commun.*, vol. 17, no. 11, pp. 7099–7115, Nov. 2018.

[34] Y. Zhang, X. Qiao, L. Yang, and H. Zhu, "Superimposed pilots are beneficial for mitigating pilot contamination in cell-free massive MIMO," *IEEE Commun. Lett.*, vol. 25, no. 1, pp. 279–283, Jan. 2021.

[35] T. C. Mai, H. Q. Ngo, and T. Q. Duong, "Downlink spectral efficiency of cell-free massive MIMO systems with multi-antenna users," *IEEE Trans. Commun.*, vol. 68, no. 8, pp. 4803–4815, Aug. 2020.

[36] W. Weichselberger, M. Herdin, H. Ozcelik, and E. Bonek, "A stochastic MIMO channel model with joint correlation of both link ends," *IEEE Trans. Wireless Commun.*, vol. 5, no. 1, pp. 90–100, Jan. 2006.

[37] X. Li, J. Zhang, Z. Wang, B. Ai, and D. W. K. Ng, "Cell-Free Massive MIMO with Multi-Antenna Users over Weichselberger Rician Channels," *IEEE Trans. Veh. Technol.*, to appear, 2022.

[38] E. Björnson and B. Ottersten, "A framework for training-based estimation in arbitrarily correlated Rician MIMO channels with Rician disturbance," *IEEE Trans. Signal Process.*, vol. 58, no. 3, pp. 1807–1820, Nov. 2010.

[39] W. Weichselberger, M. Herdin, H. Ozcelik, and E. Bonek, *Complex-valued matrix derivatives: with applications in signal processing and communications.*, Cambridge university press, 2010.

[40] Ö. Özdogan and E. Björnson and J. Zhang, "Performance of cell-free massive MIMO with Rician fading and phase-shifts," *IEEE Trans. Wireless Commun.*, vol. 18, no. 11, pp. 5299–5315, Nov. 2019.

[41] D. Tse and P. Viswanath, *Fundamentals of wireless communication*, Cambridge university press, 2005.

[42] Ö. Özdogan and E. Björnson and E. G. Larsson, "Massive MIMO with spatially correlated Rician fading channels," *IEEE Trans. Commun.*, vol. 67, no. 5, pp. 3234–3250, May. 2019.

Qiang Sun (Member, IEEE) received the Ph.D. degree in communications and information systems from Southeast University, Nanjing, China, in 2014. He was a Visiting Scholar with the University of Delaware, Newark, DE, USA, in 2016. Dr. Sun was with Technical Program Committee member and reviewer for a number of IEEE conferences/journals.He is currently a Professor with the School of Information Science and Technology, Nantong, China. His research interests include deep learning and wireless communications.

Xiaodi Ji is currently pursuing the M.S. degree in Information Science and Technology with Nantong University, China. Her research interests include performance analysis of wireless communication systems.

Zhe Wang received the B.S. degree from the College of Electronic Information, Qingdao University, Qingdao, China, in 2020. He is currently pursuing the Ph.D. degree with Beijing Jiaotong University, Beijing, China. His research interests include massive MIMO systems, signal processing, and performance analysis of wireless systems.

Xiaomin Chen received the B.S. and the M.S. degrees in communications engineering from Tongji University, Shanghai, China, in 2005 and 2008, respectively. She received her Ph.D. degree with honor in Electronic Engineering from Technische Universität Braunschweig, Germany in 2014. She is currently with the School of Information Science and Technology, Nantong University, Nantong, China. Her research interests include error-control coding, wireless networks and machine learning in communication systems.

Yongjie Yang was born in Nantong, Jiangsu, China, in 1969. He received the B.Sc. degree in automation from the Nantong Institute of Technology, Nantong, in 1994, and the M.S. degree in communication and information system from the Nanjing University of Science and Technology, Nanjing, China, in 2002.,Since 1994, he has been with Nantong University, Jiangsu, where he is currently a Professor. He has authored or coauthored more than 50 international journal or conference papers. He holds more than ten Chinese patents. His current research interests include intelligent control, embedded systems, and wireless communications.

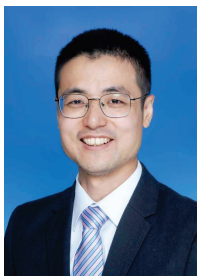

Jiayi Zhang (S'08–M'14–SM'20) received the B.Sc. and Ph.D. degree of Communication Engineering from Beijing Jiaotong University, China in 2007 and 2014, respectively. Since 2016, he has been a Professor with School of Electronic and Information Engineering, Beijing Jiaotong University, China. From 2014 to 2016, he was a Postdoctoral Research Associate with the Department of Electronic Engineering, Tsinghua University, China. From 2014 to 2015, he was also a Humboldt Research Fellow in Institute for Digital Communications, Friedrich-Alexander-University Erlangen-Nurnberg (FAU), Germany. From 2012 to ¨ 2013, he was a visiting scholar at the Wireless Group, University of Southampton, United Kingdom. His current research interests include massive MIMO, large intelligent surface, communication theory and applied mathematics. Dr. Zhang received the Best Paper Awards at the WCSP 2017 and IEEE APCC 2017. He was recognized as an exemplary reviewer of the IEEE COMMUNICATIONS LETTERS in 2015 and 2016. He was also recognized as an exemplary reviewer of the IEEE TRANSACTIONS ON COMMUNICATIONS in 2017-2019. He was the Lead Guest Editor of the special issue on "Multiple Antenna Technologies for Beyond 5G" of the IEEE JOURNAL ON SELECTED AREAS IN COMMUNICATIONS in 2020. He currently serves as an Associate Editor for IEEE TRANSACTIONS ON COMMUNICATIONS, IEEE COMMUNICATIONS LETTERS, IEEE ACCESS and IET COMMUNICATIONS.

Kai-Kit Wong (M'01-SM'08-F'16) received the BEng, the MPhil, and the PhD degrees, all in Electrical and Electronic Engineering, from the Hong Kong University of Science and Technology, Hong Kong, in 1996, 1998, and 2001, respectively. After graduation, he took up academic and research positions at the University of Hong Kong, Lucent Technologies, Bell-Labs, Holmdel, the Smart Antennas Research Group of Stanford University, and the University of Hull, UK. He is Chair in Wireless Communications at the Department of Electronic and Electrical Engineering, University College London, UK. His current research centers around 5G and beyond mobile communications. He is one of the early researchers who proposed multiuser MIMO. His paper published in WCNC 2000 marked the first ever research work on multiuser MIMO in the field. He is Fellow of IEEE and IET and is also on the editorial board of several international journals. He is the Editor-in-Chief for IEEE Wireless Communications Letters since 2020.